A Study of Rough Surface Scattering Phenomena

in the LMDS Band (28 GHz)

By

Cindy Lin Dillard
(Chin-Yau Lin)

Thesis submitted to the Faculty of the
Virginia Polytechnic Institute and State University
in partial fulfillment of the requirements for the degree of

Master of Science
in
Electrical Engineering

Charles W. Bostian, Chairman
Scott F. Midkiff
Dennis G. Sweeney

February 27, 2003
Blacksburg, Virginia

Keywords: LMDS, Scattering, Radio wave propagation, 28 GHz, Rough surface.

A Study of Rough Surface Scattering Phenomena in the LMDS Band (28 GHz)

Cindy Lin Dillard

(ABSTRACT)

In this study, the properties of the reflected paths and scattering phenomena were investigated in the LMDS band (28 GHz). We used the newly developed sampling swept time delay short pulse (SSTDSP) sounder to collect field data in certain locations on the Virginia Tech campus. The sounder collected the channel impulse response analog waveform, sampled, digitized and reconstructed it. The stored data were used to produce the power delay profile and other channel parameters. In particular, we collected scattered and reflected data regarding the channel response with different incident angle and distance set-ups from brick and limestone walls. We used the reflected pulse width and maximum excess delay derived from each power delay profile to analyze the rough surface scattering phenomena. We found that limestone and brick walls exhibited some diffuse scattering. The reflected pulse of a limestone wall had more maximum excess delay spread than did a brick wall at -15dB power threshold. The mean maximum excess delay for the reflected pulse of the limestone wall measurement set-ups was more than two times that of the brick wall. With equal transmitter and receiver distances to the wall, we found that as the incident angle increased, the maximum excess delay decreased but the perpendicular reflection coefficient increased. It is recommended that for future study, a second generation SSTDSP sounder will replicate the measurement with larger distance and angle set-ups as well as in non-line-of-sight areas.

Grant Information

This study was sponsored by NSF under grants 9983463 and 9979364 also by 2001Virginia Space Grant Consortium Aerospace Graduate Research Fellowship.

Dedication

To two most significant men in my life:

My father, Mr. Show-Yi Lin

&

My husband, Professor David A. Dillard

Acknowledgments

When I was a little girl, even though I was very good at math and physics, I never thought about becoming an engineer because girls were not encouraged to be in science or technology fields. However, I have inherited my father's genes and am destined to become an engineer sometimes in my life. Fifteen years have passed with a blink after I graduated from college. Five years ago, I started taking engineering calculus and freshman engineering courses. Every one of my engineering interests was awakened and demanded more and more knowledge in the engineering field. With two years of straight A undergraduate engineering courses, I was given an chance to work with my graduate advisor, Dr. Bostian to earn a Master's degree in Electrical Engineering. From then on my journey to become an electrical engineer has become more challenging but more satisfying.

It was not an easy journey, however, the Wonderful Counselor has brought into my life many encouraging and inspiring professors which include Dr. Lamine Mili, Dr. John Besieris, Dr. David De Wolf, Dr. Gregory Durgin, and Dr. Tim Pratt. They kept my interests in learning more and more about electrical engineering knowledge to lead me into doing my master's study.

In the process of doing my study, Dr. Sweeney taught me a lot about RF hardware in the lab. Dr. Bostian continued encouraging me when I was discouraged and frustrated with the study. In many difficult occasions, he was my source of strength. He was more than a graduate student advisor to me. My special friend Tim Gallagher helped me tremendously in developing my analytical model and

collecting data. His patience and insights sustained me in many difficult moments. Finally Dr. Midkiff did a wonderful job in editing and correcting my thesis draft.

My biggest gratitude goes to my husband, Professor Dillard who had so much unconditional love to support me in the past five years. Without him, earning this Master's degree would have been impossible for a middle-aged woman like me.

Contents

Page

Chapter 1 Introduction……1

1.1 Definition of LOS in LMDS……..…4

1.2 Spectra Reflected Waves.…….6

1.2.1 Reflection coefficients……....6

1.2.2 Two Ray Model.…….....8

1.2.3 Relating received power to electric field……..10

1.3 Scattering……11

1.3.1 Scattering loss factor……11

1.3.2 Bistatic scattering…….12

1.3.3 Radar cross section model……13

1.4 Related Studies Appling Rough Surface Loss Factor Model……..13

1.5 Conclusion……...18

Chapter 2 Channel Sounding Literature Review…….20

2.1 Sounder Characteristics……...20

2.2 Three Types of Sounders…….24

2.3 Sampling Swept Time Delay Short Pulse Sounder (SSTDSP)……...25

2.4 Studies Related to Characterize LMDS Channels……...28

2.5 Conclusion……...31

Chapter 3 Measurement Procedures and Analysis……..33

3.1 Calibration……...33

3.1.1 Impulse signal……...33

3.1.2 Outdoor calibration measurement……34

3.1.3 Antenna pattern measurement……..37

3.1.4 Calibration data analysis……..38

3.2 Reflection/Scattering Measurements on Two Kinds of Wall…….40

3.2.1 Limestone wall measurement……..41

3.2.2 Brick wall measurement……..42

3.3 Conclusion……..42

Chapter 4 Results……43

4.1 Data processing procedures……43

4.2 Analysis of power delay profile raw data……...47

4.3 Data analysis of reflection coefficients……...52

Chapter 5 Discussion……..55

5.1 Scattering phenomena…….55

5.2 Reflection coefficient……..56

5.3 The SSTMDP sounder……57

5.4 Summary of Contributions……58

5.5 Suggestions for Future Research……58

References……60

Appendix……..64

Vita……81

List of Tables

Page

Table 2.1 Summary of Result Findings in the Literature…… 32

Table 3.1 Calibration Measurement Set-ups……..……. 35

Table 3.2 Calibration Data…..…… 39

Table 3.3 Measurement Set-up……..……. 41

Table 4.1 Summary Table of Raw Data…….. 46

Table 4.2 Reflection Coefficients……..……. 54

Table 5.1 Perpendicular Reflection Coefficient($\Gamma_{\perp}$) Study Comparison…… 57

Table A.1 Medium Parameters…… 71

Table A.2 Comparison of Measured and Simulated Excess Pulse Duration…..…. 73

List of Figures

Page

Figure 1.1 Point to multipoint layout…… 2

Figure 1.2 Mesh layout…….. 2

Figure 1.3 Fresnel geometry…….. 4

Figure 1.4 First Fresnel zone……. 5

Figure 1.5 Incident E-field and reflected E-field……... 7

Figure 1.6 Ground reflection……. 9

Figure 2.1 LMDS channel as a two port network……21

Figure 2.2 Channel impulse response for a LOS signal and specular reflections…22

Figure 2.3 SSTDSP system block diagram……. 27

Figure 2.4 Transmit pulses and received channel response…… 28

Figure 3.1 Channel impulse response obtained by the SSTDMP……34

Figure 3.2 Calibration reflector……... 35

Figure 3.3 LOS pulse and reflected pulse……... 36

Figure 3.4 Antenna pattern measurement set-up…… 37

Figure 3.5 Antenna pattern……. 38

Figure 3.6 Limestone wall and brick wall used in the study…….. 40

Figure 3.7 Measurement set-up…….. 42

Figure 4.1 Raw data and envelop of the absolute value display……. 44

Figure 4.2 Power delay profile (10.3.9.1)……... 44

Figure 4.3 Comparison of limestone/brick power delay profiles…… 45

Figure 4.4 LOS pulse power profile…… 47

Figure 4.5 -3dB excess pulse duration…… 48

Figure 4.6 -10dB excess pulse duration…….. 48

Figure 4.7 Maximum excess delay at –15 dB……. 49

Figure 4.8 Excess delay for equal distance set-up (9m)……. 49

Figure 4.9 Excess delay for equal distance set-up (6m)……. 50

Figure 4.10 Maximum excess delay and incident angle comparison (limestone).. 51

Figure 4.11 Maximum excess delay and incident angle comparison (brick)……. 51

Figure 4.12 Brick reflection coefficient (perpendicularly polarized)……. 53

Figure 4.13 Limestone reflection coefficient (perpendicularly polarized)……. 53

Figure A.1 Lobe shaped E-field…….. 64

Figure A.2 Scattered E-field……... 65

Figure A.3 Exponential n power……. 66

Figure A.4 Fresnel reflection zones (n= up to 15)..…… 67

Figure A.5 Fresnel reflection zone geometry….……. 68

Figure A.6 Power delay profile with n=0.8 for scattered E-field……... 72

Figure A.7 Excess pulse width duration comparison (brick).……. 74

Figure A.8 Excess pulse width duration comparison (limestone)…….. 74

Chapter 1 Introduction

Local multipoint distribution service (LMDS), a broadband wireless service, began in the U. S. when the Federal Communications Commission (FCC) auctioned the unused 1300 MHz spectrum in the 27 to 31 GHz band in 1998. The US band is 27.5-28.35 GHz, 29.1-29.25 GHz, and 31.075-31.225 GHz. In Europe, the band is from 40.5 to 43.5 GHz. LMDS technology is now in its first stage of implementation and is expected to enhance development of broadband service [1]. As long as line of sight (LOS) paths exist, LMDS can be used for high data rate information transmission, television broadcasting, video streaming, Internet browsing, two-way wireless communication, etc.

LMDS can operate in a point-to-point, point-to-multipoint, or mesh layout (see Figure 1.1 and Figure 1.2 for examples). The point-to-point system includes one hub and one remote unit. The point-to-multipoint system (Figure 1.1) requires a hub and a group of remotes that communicate directly with the hub. The transmitter hub and the receiver in the remote site can typically be separated by 2 to 5 km. Usually in deployment the transmitter and receiver sites need to be in line-of-sight (LOS). Normally, the transmitter antenna is on top of a tall building or on a high pole overlooking the service area. The transmitting antenna sector usually covers an integer fraction of 360°. The narrower the antenna beam used, the longer the range that the transmitter can cover. The hub site can be connected to a local exchange carrier (LEC) network with fiber links such as OC3, OC12, or others. The remote site receiver can be connected with Ethernet and/or wireless local area network (LAN) access point to the users.

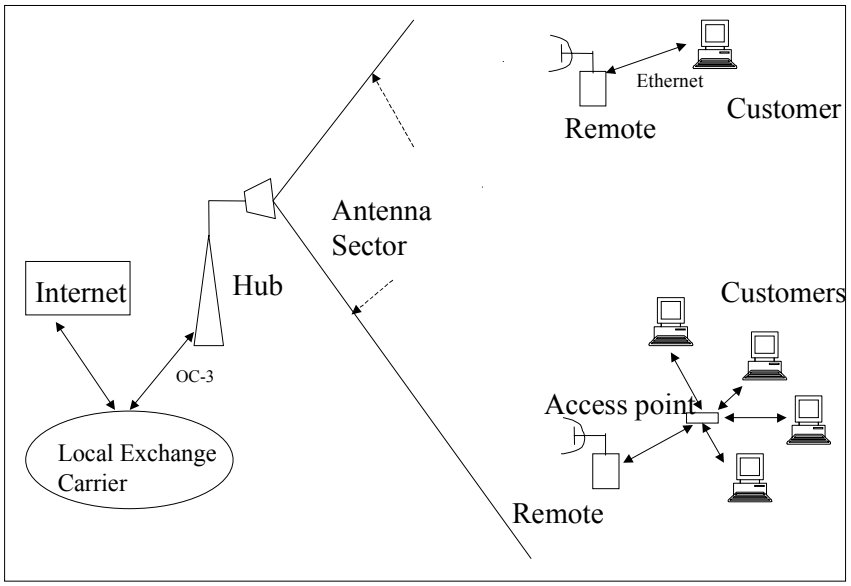

Figure 1.1 Point to multipoint layout

The mesh design (Figure 1.2) is used to overcome possible line of sight problems. This design is especially suitable for users that are located on a street that stretches for a far distance that the hub transceiver may not be able to reach. Mesh systems do not require a hub station; instead nodes are connected by point-to-point

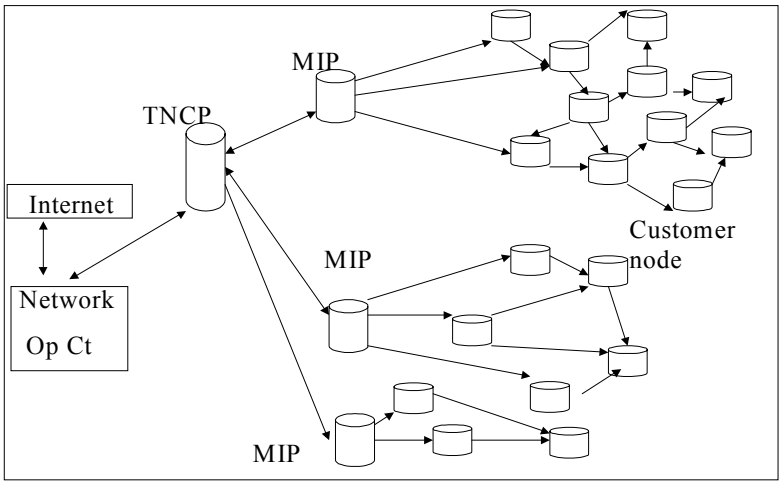

Figure 1.2 Mesh layout

radio links to other nodes. Nodes can transmit and receive data to and from other nodes. A trunk network connection point (TNCP) is connected to the networking operations center then link to the Internet. A mesh insertion point (MIP) is connected between TNCP and customer nodes. As described in Figure 1.2, the mesh layout design has each customer node connected to at least two other nodes. If necessary, a dummy seed node will be provided. Mesh technology is still in the experimental stage and, therefore, it is not yet operated widely in the United States.

As mentioned earlier, LMDS radio needs to operate in LOS. Commercially the coverage rate, defined as the ratio of the number of actual subscribers to the total number of potential subscribers that can receive the transmitted signal can be around 60% to 70% [2]. Many studies have focused on methods of enhancing the coverage rate. The literature shows that using repeaters or reflectors can enhance the coverage; raising antenna height can also enhance the coverage [2]. Some researchers have pointed out that reflected waves can be used in the non-line-of-sight (NLOS) areas. However, the signal strengths and dispersion characteristics of the reflected signals have not been fully described.

In this study, we have investigated the properties of the reflected paths and scattering. We used the sampling swept time delay short pulse (SSTDSP) sounder [16] to map the channel characteristics in certain locations on the Virginia Tech campus. In particular, we collected scattered and reflected signal data regarding the channel response with different incident angle and distance set-ups from two types of wall, brick and limestone. From the sounder measurements, we determined power delay profiles for all set-ups. With these, we hope to be able to contribute to

the understanding of LMDS channel response characteristics when signals scatter and reflect from different types of wall.

1.1 Definition of LOS in LMDS

Line of sight in radio propagation is usually defined by being obstruction free within the first Fresnel zone. According to Rappaport, "A rule of thumb used for design of line-of-sight microwave links is that as long as 55% of the first Fresnel zone is kept clear, then further Fresnel zone clearance does not significantly alter the

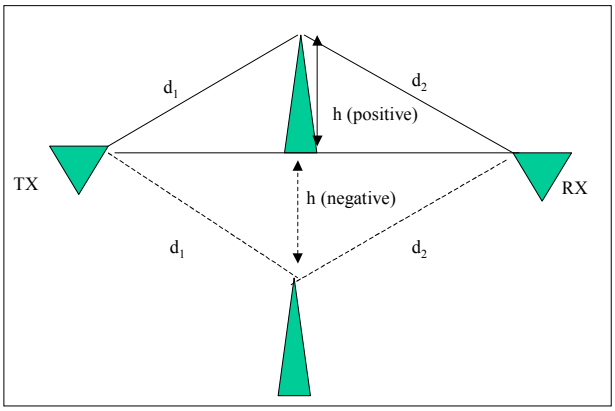

Figure 1.3 Fresnel geometry

diffraction loss." [3]

Figure 1.3 shows the Fresnel geometry. A knife-edge obstacle of height *h* blocks the radio path. The distance between the transmitter to the top of the obstacle is d1 and the distance between the receiver to the top of the obstacle is *d2*. The

difference in distance between the direct path and the diffracted length, also called excess path length, can be approximated by

$$\Delta d = \frac{h^2(d_1 + d_2)}{2d_1 d_2} \tag{1.1}$$

The dimensionless Fresnel-Kirchoff diffraction parameter which can be used to calculate the loss due to diffraction over a knife-edge obstacle is given by [4]

$$v = h\sqrt{\frac{2(d_1 + d_2)}{\lambda d_1 d_2}} \tag{1.2}$$

The first Fresnel zone encloses all radio paths for which the additional path length does not exceed half of the wavelength. The second Fresnel zone encloses all paths for which the additional path does not exceed one wavelength and so on. By setting Δd to $\lambda/2$, and changing the obstruction height, h, to the Fresnel radius, F,

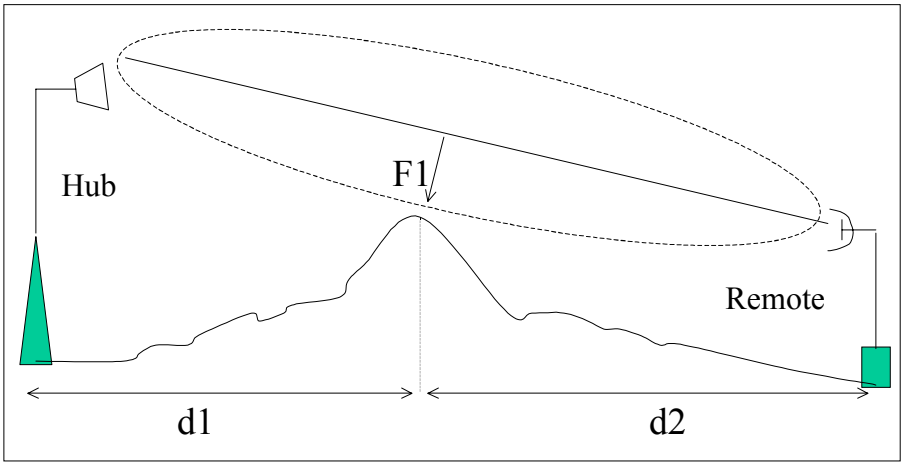

Figure 1.4 First Fresnel zone

and solving for F, the first order Fresnel zone radius [4] can be expressed as:

$$F_1 = 17.3\sqrt{\frac{d_1 d_2}{f(d_1 + d_2)}} \tag{1.3}$$

with F_1 is the ellipse radius in meters of the three-dimensional first Fresnel zone, f is frequency in GHz, d_1 and d_2 are distances in km from transmitter and receiver to the obstructive object (see Figure 1.4).

1.2 Specular Reflected Waves

In areas that LOS does not exist, radio paths are called shadowed. Shadowing is caused by vegetation, buildings, or other objects blocking the path between the transmitter and the receiver. Radio waves that cannot go from the transmitter site to the receiver site directly may bounce and cause signals to arrive at delayed times. The radio wave can be reflected, scattered, or absorbed by the various objects it meets. Many studies have pointed out that the reflected waves may be useful in the shadowed areas. In this section, we discuss the basics of reflected waves, as well as two ray model and ground reflection models used to describe the received signals.

1.2.1 Reflection coefficients

Knowing the angle of incidence (θ) and polarization of the wave, along with the electrical properties of the media, the reflected wave can be characterized. The reflection coefficients [5] involves material properties such as intrinsic impedance

(η) and refraction index (n), as well as path properties incidence angle (θ_i) and transmitted angle (θ_t), and is given by:

$$\Gamma_{\parallel} = \frac{E_r}{E_i} = \frac{\eta_2 \cos\theta_t - \eta_1 \cos\theta_i}{\eta_2 \cos\theta_t + \eta_1 \cos\theta_i} \tag{1.4}$$

$$\Gamma_{\perp} = \frac{E_r}{E_i} = \frac{\eta_2 \cos\theta_i - \eta_1 \cos\theta_t}{\eta_2 \cos\theta_i + \eta_1 \cos\theta_t} \tag{1.5}$$

where the intrinsic impedance for a general medium is defined by its parameters of permeability (μ), permittivity (ϵ), conductivity (σ) and angular frequency of the wave (ω):

$$\eta = \sqrt{\frac{j\omega\mu}{\sigma + j\omega\varepsilon}} \tag{1.6}$$

The incident E-field can be decomposed into two parts, perpendicular and

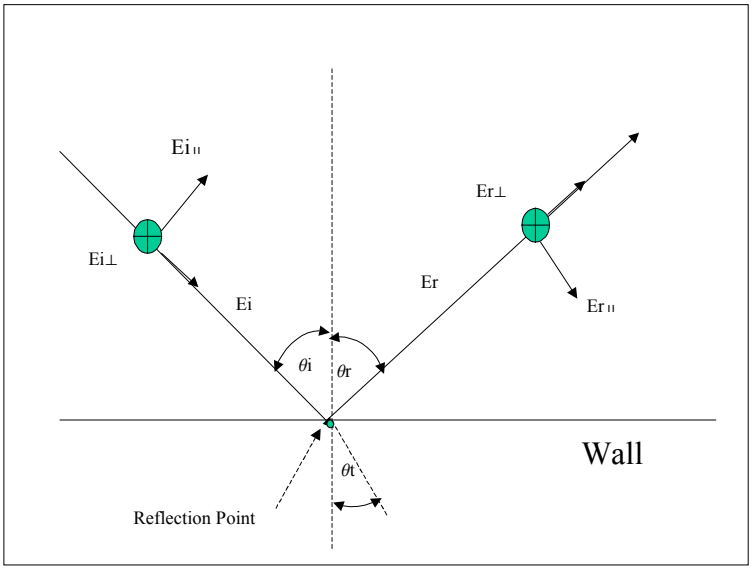

Figure 1.5 Incident E-field and reflected E-field

parallel components as shown in Figure 1.5. In the case of perpendicular polarization, E_i is perpendicular to the plane of incidence, the plane containing the direction of propagation of the incident wave and the normal to the boundary surface. The perpendicular reflection coefficient is indicated as $\Gamma_{\perp}$. Perpendicular polarization is also referred as horizontal polarization or E-polarization. In the case of parallel polarization, E_i is parallel to the plane of incidence. The parallel reflection coefficient is indicated as $\Gamma_{\parallel}$. Parallel polarization is also referred as vertical polarization or H-polarization. Reflection coefficients are complex quantities that represent the magnitude and phase change of the E-field components at the interface medium. These changes are responsible for depolarization.

From the above equations, for free space $\eta_1 = \eta_0 = 120\pi$, refraction index, n_1=1, and $n_1/n_2=\eta_2/\eta_1$. Therefore, the reflection coefficients can be expressed as:

$$\Gamma_{\parallel} = \frac{E_r}{E_i} = \frac{\sqrt{n_2^2 - \sin^2\theta_i} - n_2^2\cos\theta_i}{\sqrt{n_2^2 - \sin^2\theta_i} + n_2^2\cos\theta_i} \tag{1.7}$$

$$\Gamma_{\perp} = \frac{E_r}{E_i} = \frac{\cos\theta_i - \sqrt{n_2^2 - \sin^2\theta_i}}{\cos\theta_i + \sqrt{n_2^2 - \sin^2\theta_i}} \tag{1.8}$$

1.2.2 Two ray model

The two ray model is normally used to describe ground reflection phenomena in the radio channel. The model consists of a LOS electric field (E-field), and a reflected E-field. Depending on the polarization, the reflected E-field is the incident E-field multiplied by the reflection coefficient and the reflected angle is the same as the incident angle (Figure 1.6).

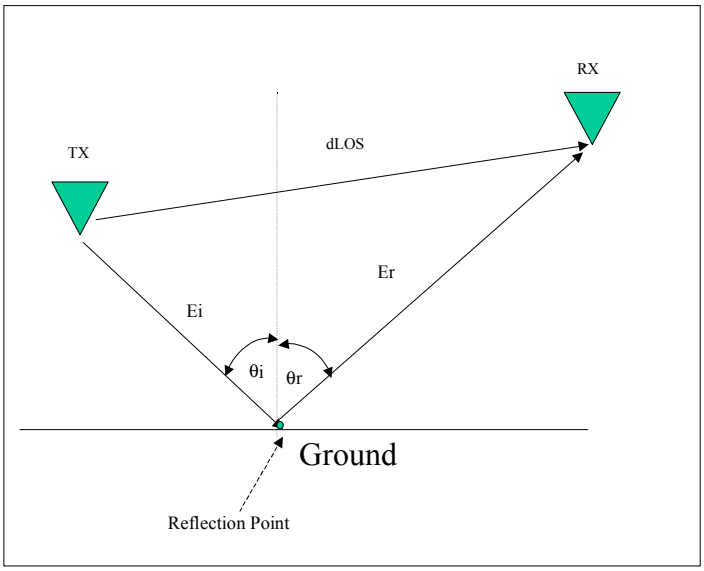

Figure 1.6 Ground reflection

If a two ray ground reflection model is assumed, the total E-field received will be the sum of the LOS E-field and the E-field of the ground reflected component:

$$E_{total} = E_{los} + E_g \tag{1.9}$$

The reflection properties of a smooth surface are characterized by a complex reflection coefficient. For perpendicular polarization, the complex reflection coefficient [4] is expressed as:

$$\Gamma_{\perp} = \frac{\sin\theta - \sqrt{(\varepsilon_r - jx) - \cos^2\theta}}{\sin\theta + \sqrt{(\varepsilon_r - jx) - \cos^2\theta}} \tag{1.10}$$

where incident angle θ is defined as from ground plane to the incident wave.

For parallel polarization, the complex reflection coefficient is given as:

$$\Gamma_{\parallel} = \frac{(\varepsilon_r - jx)\sin\theta - \sqrt{(\varepsilon_r - jx) - \cos^2\theta}}{(\varepsilon_r - jx)\sin\theta + \sqrt{(\varepsilon_r - jx) - \cos^2\theta}} \tag{1.11}$$

where ε_r is the relative dielectric constant of the ground, x is given by 18 x 10^9 σ/f, σ is the conductivity of the medium in S/m and f is the frequency in Hz. Bacon [4] points out that "for grazing incidence, (incident angle as 90°) the reflection coefficient for both polarizations tends to –1 therefore unity amplitude and the phase are reversed and there tends to be little difference between the two polarizations as far as reflection from smooth ground is concerned. However, this does not apply to reflection from buildings, where large incidence angles are common." It also would not apply to buildings that are rough on a scale of wavelength. The ground reflected E field is the product of the reflection coefficient and the incident E-field measured at a certain distance from the transmitter.

1.2.3 Relating received power to electric field

With parameters such as received E-field, operating frequency, distance, transmitter and receiver antenna height above ground, and receiver antenna effective aperture as well as gain, the received power can be obtained with the equation as follows [3,6]:

$$P_r(d) = P_d A_e = \frac{|E|^2}{120\pi} A_e = \frac{|E|^2}{120\pi} \frac{Gr\lambda^2}{4\pi} = \frac{P_t G_t G_r \lambda^2}{(4\pi)^2 d^2} \tag{1.12}$$

with P_d as the power flux density in free space. E is the total received electric field, which may include both LOS E-field and reflected E-fields. This equation is known

as the Friis transmission equation [6] and is essential in calculating power received in any radio link.

1.3 Scattering

In this section, three significant aspects of scattering phenomena are summarized: the scattering loss factor, bystatic scattering, and radar cross section model.

1.3.1 Scattering loss factor

Reflection ceases to be specular if the spread in path lengths between the antennas via different points on the surface exceeds λ/4. This is the Rayleigh criterion of surface roughness according to Livingston [7]. Later, however, the Rayleigh criterion used as a test for surface roughness was redefined [8]. The critical height (h_c) of surface protuberances is defined as

$$h_c = \frac{\lambda}{8\cos\theta_i} \tag{1.13}$$

where λ is the RF wavelength, and the peak-to-peak height (h) defined as the minimum to maximum surface protuberance. A surface is considered as rough if $h > h_c$. At the 28 GHz LMDS band, the wavelength is about 1 cm. If the incident angle is 5°, the critical height is 1 mm. If the incident angle is 60°, h_c is 2.7 cm. Therefore, based on this criterion, almost any building surface can be considered rough for 28 GHz. It is therefore important to investigate rough surface scattering phenomena.

When a surface is rough, a scattering loss factor is introduced to account for diminished energy in the specular direction of reflection. The scattering loss factor was first derived by Ament [9] as

$$\rho_s = \exp[-8(\frac{\pi\sigma_h \cos\theta_i}{\lambda})^2] \qquad (1.14)$$

where σ_h is the standard deviation of the surface height about the mean surface height in the first Fresnel zone of the illuminating antenna. The assumption is that the surface heights are Gaussian distributed. The scattering loss factor was further modified by Boithias [8] as

$$\rho_s = \exp[-8(\frac{\pi\sigma_h \cos\theta_i}{\lambda})^2] I_0[8(\frac{\pi\sigma_h \cos\theta_i}{\lambda})^2] \qquad (1.15)$$

where I_0 is the modified Bessel function of zeroth order. When the Bessel function argument is small, the modified factor is approximately equal to the original factor.

The scattering loss factor is used to modify the reflection coefficients:

$$\Gamma_{\|rough} = \Gamma_{\|} \cdot \rho_s \qquad (1.16)$$

$$\Gamma_{\perp rough} = \Gamma_{\perp} \cdot \rho_s \qquad (1.17)$$

These reflected E-fields are calculated by multiplying the modified reflection coefficients by the incident E-fields.

1.3.2 Bistatic scattering

Bistatic scattering by a rectangular conducting plate is well understood and will be useful later in this thesis as a frame of reference. If the reflector is a

rectangular conducting plate in free space, the distant back-scattered field is given by [4]

$$E = \frac{-jkE_o A}{2\pi r} e^{-jkr} \tag{1.18}$$

where A is the area of the plate and r is the distance from the plate to the point of observation.

1.3.3 Radar cross section model

In radio channel where large, distant objects induce scattering, with E-field described in Equation 1.18, the received power can be calculated using the following equation [4,10]:

$$\Pr = \frac{PtGtGrA\lambda^2}{(4\pi)^3 (d_t d_r)^2} \tag{1.19}$$

where d_t and d_r are the distance from the scattering object to the transmitter and receiver, respectively, and A in m^2 is the effective area that all incident energy falls upon isotropically [4].

1.4 Related Studies Appling Rough Surface Loss Factor Model

Few studies related to reflected and scattered waves in the LMDS bands have been conducted. In a recent study by Hayn, Rose and Jakoby [11], reflection and multipath effects in 42 GHz LMDS radio propagation areas were modeled. The researchers compared the theoretical reflection loss and the measured reflection losses for glass, concrete and wood surfaces. The theoretical reflection loss was

calculated with modified Fresnel reflection coefficients. The experimental measurements were conducted with transmitter/receiver set-ups in an actual path with a building wall or roof as the reflector. Reflection measurements were compared with the theoretical reflection coefficients, which were the Fresnel reflection coefficients multiplied by the modified scattering loss factor like those computed from Equations 1.16 and 1.17. They found that 5 dB loss due to some measurement uncertainties could occur for concrete and wood. However, the measurement results indicated that the received reflected power in areas of the buildings with smooth windowpanes and metallic window frames had relatively low reflection losses, thus the measured power levels were higher compared to the predicted values. They concluded that the relatively strong reflections could be used to enhance the area coverage in the NLOS areas when the system margin is sufficient. The researchers suggested that the use of elliptical reflectors as passive repeaters was a reliable option to enhance coverage in shadowed areas.

In Hayn, Rose and Jakoby's study, the total field strength was calculated by taking into account the polarization mismatch with the receiving antenna and the free space attenuation. All measured power levels were several dB above the predicted values. The researchers concluded that the maximum received power is often caused by areas of the buildings with smooth window panes and metallic window frames, having relatively low reflection losses and thus increasing the measured power levels compared with those predicted assuming purely concrete with rough surfaces. The study concludes that in NLOS areas, relatively strong reflections could be used, in principle, to enhance the area coverage.

A study done by Landron, Feuerstein, and Rappaport [12,13] also used the rough surface scattering loss factor to adjust the Fresnel reflection coefficients. The study was conducted at 1.9 GHz and 4.0 GHz for a variety of typical smooth and rough exterior building surfaces. Measured reflection coefficients were compared to theoretical Fresnel reflection coefficients. A wideband spread-spectrum sliding correlator system was developed by the researchers and used to collect data in this study. At the transmitter, a continuous wave (CW) source was modulated by the maximum length pseudonoise (PN) sequence. The signal was then amplified and transmitted via a high gain horn antenna. At the receiver, the signal was correlated to the identical PN sequence with a clock rate which was slightly offset from the transmitter. The baseband output was displayed in real time on the digital storage oscilloscope and stored on a computer for later processing. Ten LOS channel impulse responses with the two antennas facing each other as well as 10 reflected channel impulse responses were collected with the antennas aiming at the reflection point on the test surface.

In the post processing process, for each transmitter and receiver location, the ensemble average of the ten raw power delay profiles was calculated. The LOS power from the average LOS delay profile was taken to be the free space value:

$$(P_R)_{los} = \frac{P_t G_t G_r \lambda^2}{(4\pi d_{los})^2} \tag{1.20}$$

The averaged reflected power delay profile for the reflected path measurement was calculated as:

$$(P_R)_{ref} = \frac{P_t G_t G_r \lambda^2}{(4\pi)^2 (d_1 + d_2)^2} |\Gamma|^2 \tag{1.21}$$

where transmitter distance (d_1) was selected to ensure that incident waves striking the test surface could be approximated as plane waves. Solving for the empirical reflection coefficient yields

$$|\Gamma| = \frac{d_1 + d_2}{d_{los}} \sqrt{\frac{(P_R)_{ref}}{(P_R)_{los}}} \tag{1.22}$$

With this equation each measured reflection coefficient was obtained by averaging 10 LOS and 10 reflected path power delay profiles for limestone, glass, and brick walls at 1.9 GHz or 4 GHz. Results show that at 1.9 GHz, on the limestone wall, 90% of the measured reflection coefficients were bounded by the Fresnel formulas for smooth and rough surfaces. Modified Gaussian rough surface reflection coefficients gave better agreement with measured values. At 4 GHz, the results seemed to be identical. However, according to the results, the calculated values tended to give pessimistic predictions of the measured reflection coefficient values. The authors concluded that the calculated scattering loss factor perhaps overestimated the scattering loss. This might be attributed to the simplifying assumptions such as Gaussian distribution of surface heights, sharp edge effects, etc. in the calculated scatting loss factor. The significant variability can also be attributed to ground reflection effects and interference of the reflected multipath due to surface protuberances. Furthermore, the authors proposed a model to calculate the reflection coefficients for smooth and rough surfaces as a function of incidence angle:

$$\Gamma_{ave} = (\frac{1+\rho_s}{2})\Gamma_{\|,\perp} \tag{1.23}$$

where $\Gamma_{\|,\perp}$ is either the parallel or perpendicular polarization reflection coefficient and ρ_s is the scattering loss factor.

For the glass walls, at 4.0 GHz, the measured coefficients closely agreed with the theoretical Fresnel reflection coefficients using σ = 2.5 S/m. For brick wall results at 4.0 GHz, the differences between the theoretical models of the smooth versus rough surface are much smaller than in the rough limestone case. The measured values are more similar as the predicted smooth surface coefficients though. This is due to the reflection being predominantly specular.

Kim, Yang, and Kim [14] have also conducted a study of scattering characteristics of surface roughness at LMDS frequency bands. The reflection characteristics of materials were measured using a vector network analyzer. The complex refractive index of cement block was deduced as n=2.2443-j0.0597 from the experimental data using a nonlinear least square method. The reflection coefficients were measured for three types of cement block wall in the frequency range from 26.5 GHz to 40 GHz. at incidence angles from 5^o to 70^o. For parallel polarization, the reflection curves in all three types of wall showed similar characteristic to plane surfaces. For perpendicular polarization, the reflection coefficients showed very irregular character. Depending on the incidence angle, the scattering can be increased. At 65^o, for perpendicular polarization, the coefficients were almost the maximum but for parallel polarization they were the minimum for 28 GHz.

Regarding possibilities of using the reflective wave in NLOS at the 28 GHz band, Seidel and Arnold [15] used a vertically polarized Cellular Vision broadcast signal as the transmitted signal source, and received signal strength was measured with a custom receiver at antenna heights ranging from 3.4 m to 11.3 m above ground level. Specular reflections were investigated by sweeping the directional receiver antenna through 360° azimuth at a fixed elevation angle parallel to the ground. They pointed out that the antenna azimuth angle and receiver antenna height would affect coverage. There also existed special cases where stronger signals are received via reflection than from the direct path. The researchers concluded that specular reflections might potentially be used in NLOS areas. In their measurement the dominant signal arrived via specular reflections at less than 10% of the 77 co-polarized measurement locations.

1.5 Conclusion

1.1 In the literature review above, the focus of all studies seemed to relate to the changes of signal strength in reflection. However, how the signal was dispersed in space and how the signal was spread in time domain were not described in detail in most of the studies. According to the literature review, the rough surface factor model seems to be a reasonable model for establishing a analytical model to investigate rough surface scattering phenomenon. In the two ray model however, the fact that reflection surface could be rough is neglected and rough surface scattering phenomena are simply overlooked. The radar cross section model can also be integrated in the simulation model to describe the LMDS band scattering phenomena. The author has attempted to develop a model to describe the scattering

model for LMDS band, however there are still many issues waiting to be resolved. The preliminary model is described in Appendix A.

Chapter 2 Channel Sounding Literature Review

In radio engineering, channel refers to the space between the transmitter and receiver. The channel acts like a filter through which the transmitted signal passes in order to reach the receiver. Even when a LOS path exists, multipath transmission still occurs due to reflections from the ground and surrounding structures. Commercially or in other applications, LMDS providers/users normally use trial and error to find the best locations for the hub and remote, a time consuming and inefficient method. If sounding the channel is possible, it will save time and energy to find appropriate locations for the hub and remote. Therefore, developing sounder techniques to characterize and optimize the channel is very significant, especially when time is limited such as in disaster rescue or military applications.

In this chapter, the theory behind sounding channel, measurement parameters/models, and varieties of sounders will be described. A section will be devoted to discuss the recent studies that are related to LMDS channel sounding.

2.1 Sounder Characteristics

The general radio channel is a time-variant two-port network. Mathematical parameters of the wideband channel are used to describe the channel characteristics. The radio channel is treated as a two port network. Whether the system is time-variant or time-invariant depends on whether the transmitter and receiver are stationary or not. Since LMDS hub and remote are usually fixed, the LMDS channel is treated as time invariant. The transmitted and received signals are treated as input and output while the channel may be represented as a transfer function (Figure 2.1).

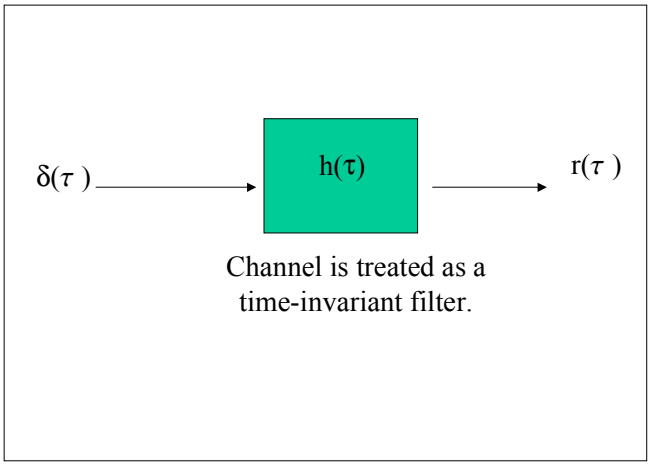

Figure 2.1 LMDS channel as a two- port network

The wideband signal may be an impulse function. When the reflection is discrete and specular, the channel response is expressed as:

$$h(t,\tau)=\sum_{i=0}^{N-1}a_i(t,\tau)\exp[\,j(2\pi\, f_c\tau_i(t)+\phi_i(t,\tau))]\delta(\tau-\tau_i(t)) \qquad (2.1)$$

where $a_i(t,\tau)$ and $\tau_i(t)$ are the real amplitudes and time delay, respectively, of the i^{th} multipath component at time t. $2\pi f_c\tau_i(t)+\phi_i(t,\tau)$ represents the phase shift due to free space propagation of the i^{th} multipath component, plus any additional phase shifts, which are encountered in the channel. If the channel impulse response is assumed to be time invariant, the channel impulse response in discrete form can be simplified as (Figure 2.2)

$$h(\tau)=\sum_{i=0}^{N-1}a_i\exp[\,j\theta_i]\delta(\tau-\tau_i) \qquad (2.2)$$

with τ as the delay time. For diffuse scattering, each discrete impulse response will look like a continuous waveform. Several parameters can be derived from the channel impulse response.

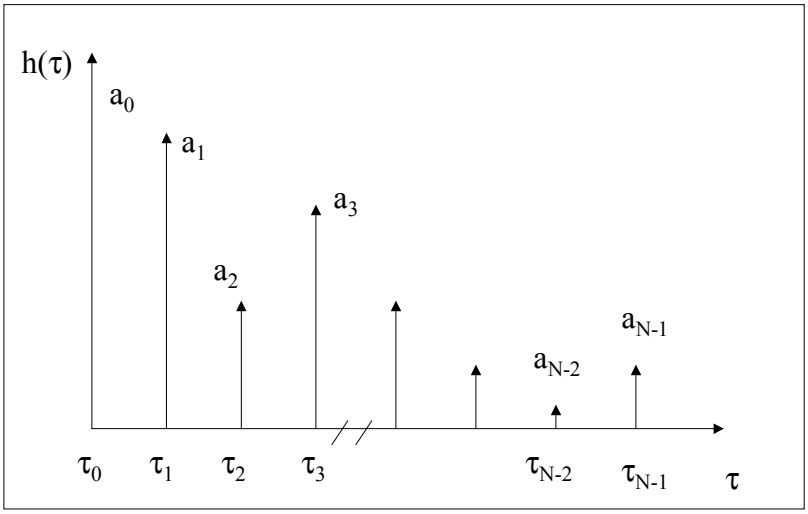

Figure 2.2 Channel impulse response for a LOS signal and specular reflections

1) Power delay profile is the spatial average of the square of the absolute value of $h(\tau)$ over a local area. This averaged value is typically derived from many snapshots of $h(\tau)$ in a local area to provide a single time-invariant power delay profile.

$$P(\tau) = k\left|h(\tau)\right|^2 \tag{2.3}$$

2) The mean excess delay value is the "average" multipath delay and is the first moment of the power delay profile. It is defined to be

$$\bar{\tau} = \frac{\sum_k a_k{}^2 \tau_k}{\sum_k a_k{}^2} = \frac{\sum_k p(\tau_k)\tau_k}{\sum_k p(\tau_k)} \tag{2.4}$$

3) The RMS delay spread is the square root of the second central moment of the power delay profile:

$$\sigma_\tau = \sqrt{\left(\overline{\tau^2} - \bar{\tau}^2\right)} \tag{2.5}$$

where

$$\overline{\tau^2} = \frac{\sum_k a_k{}^2 \tau_k{}^2}{\sum_k a_k{}^2} = \frac{\sum_k p(\tau_k)\tau_k{}^2}{\sum_k p(\tau_k)}$$

4) For a given multipath threshold *X* dB of the power delay profile, the maximum excess delay is defined as the time delay during which the energy of the measured multipath component falls *X* dB below the peak value of the power delay profile. Mathematically this value can be expressed as $\tau_x - \tau_0$ where τ_0 is the first arriving signal and τ_x is the maximum delay at which a multipath component is no more than *X* dB down from the strongest arriving multipath component.

5). The coherence bandwidth is a statistical measure of the range of frequencies over which the channel response has approximately equal gain and linear phase, or the bandwidth over which the frequencies are correlated [3]. The coherence bandwidth can be related to the RMS delay spread for correlation coefficients of 0.5 to 0.9 and can be represented as

$$\frac{1}{50}\sigma_\tau < B_c < \frac{1}{5}\sigma_\tau$$

2.2 Three Types of Sounders

Three kinds of sounders used to measure channel characteristics have been described [3]:

1) Direct RF pulse system: a repetitive pulse is transmitted and a receiver with a wide bandpass filter is used. The received signal is then amplified, detected and displayed and stored on a high speed oscilloscope.

Rappaport [3] points out several advantages and disadvantage of this system. The system is simple to set up, but it is subject to interference and noise due to the wide pass band filter required for multipath time resolution. Also, the phases of the individual multipath components are not received, due to the use of an envelope detector.

2) Spread spectrum sliding correlator channel sounder: The essence of the spread spectrum sliding correlator channel sounder is well summarized by Rappaport [3], "… a carrier signal is spread over a large bandwidth by mixing it with a binary pseudo-noise (PN) sequence having a chip duration T_c and a chip rate R_c equal to $1/T_c$ Hz. The spread spectrum signal is then received, filtered, and despread using a PN sequence generator identical to that used at the transmitter….The transmitter chip clock is run at a slightly faster rate than the receiver chip clock. … When the incoming signal is correlated with the receiver sequence, the signal is collapsed back to the original bandwidth, envelope detected, and displayed on an oscilloscope. Since different incoming multipaths will have different time delays, they will maximally correlate with the receiver PN sequence at different time…. After

envelope detection, the channel impulse response convolved with the pulse shape of a single chip is displayed on the oscilloscope."

Advantages and disadvantages of this sounder are pointed out by Rappaport [3]. This sounder has the ability to reject passband noise. The disadvantages may include that measurements are not made in real time, but are compiled as the PN codes slide past one another, the time required to make power delay profile measurements may be excessive and a non-coherent detector is used so that phases of individual multipath cannot be measured.

3) Frequency domain channel sounder: A synthesized frequency sweeper is controlled by a vector network and an S-parameter test set is used to monitor the frequency response of the channel. By stepping through discrete frequencies, the sweeper scans a particular frequency band. For each frequency step, the S-parameter test set transmits a known signal level at port 1 and monitors the received signal level at port 2. The analyzer is used to determine the complex response of the channel over the measure frequency range [3]. The limitations pointed out by Rappaport include: the system requires careful calibration; the system is a non-real-time measurement, not suitable for time varying impulse response measurement. Fast sweep times are necessary.

2.3 Sampling Swept Time Delay Short Pulse Sounder (SSTDSP)

Most current wireless channel sounders are based on pseudo noise (PN) coding and sliding correlator measurement. While these are effective at cellular and personal communication system (PCS) frequencies (900 MHz – 2 GHz), the

equipment is difficult to build with the needed performance at millimeter wave frequencies like 28 GHz. With support from the National Science Foundation and Motorola, Virginia Tech researchers have been developing an ultra-wideband radio based channel sounder, the sampling swept time delay short pulse (SSTDSP) sounder that may be able to measure the impulse response and the instantaneous bandwidth of the entire 850 MHz LMDS contiguous spectrum (27.5 to 28.35 GHz). This sounder is based on several technologies that together overcome previous limitations: ultra wideband (UWB) RF pulse shaping, real-time digital signal processing (DSP), geo-location and precise timing provide by the Global Positioning System (GPS), and phase lock loop (PLL). The Virginia Tech sounder technology is built into a base station and two transportable radios. All of the units include GPS receivers that precisely determine their geographic locations and report these to a geographic information system (GIS) database that includes a high-resolution map of the Virginia Tech campus (including three-dimensional representations of buildings, trees, etc.). GPS units in the transmitter and in the receiver are synchronized, and therefore have precise timing capabilities.

The block diagram [16] of the SSTDSP sounder (Figure 2.3) gives the setup of the sounder with the LMDS radio system and all other modules. The basic theory [17] behind the system is that a short pulse of sinusoidal RF carrier, which is treated as an impulse with a duration of τ_{bb} = 5 ns, is sent from the transmitter at certain repetition frequency , α (Figure 2.4) and sampled at the receiver at a sample frequency, β, which is a slightly less than α. The pulse transmit repetition period is $T_A = \frac{1}{\alpha}$. At the receiver, the sampler captures a tiny portion of the impulse response

envelope at a fixed time period, $T_B = \frac{1}{\beta}$. The tiny portion is called the bin size, $T_B - T_A$. The sounder user can arbitrarily choose bin size. The whole envelope of the channel response can be reconstructed after an elapsed time $t = N \cdot T_B$ where N is the number of pulses that must be transmitted for the receiver side to reconstruct the complete impulse response waveform. The number N is calculated by dividing the pulse transmit repetition period $T_A = \frac{1}{\alpha}$ by the bin size. For example, if we choose the transmit pulse repetition frequency, α, as 200 KHz and the sample frequency, β, as 199.995 KHz. The bin size becomes 0.125ns and N can be as big as 40000. The total time needed for sampling can be calculated as 5 ms.

After the impulse response analog waveform envelope is received, sampled, and reconstructed, it is digitized by the DSP module. The stored data is used by

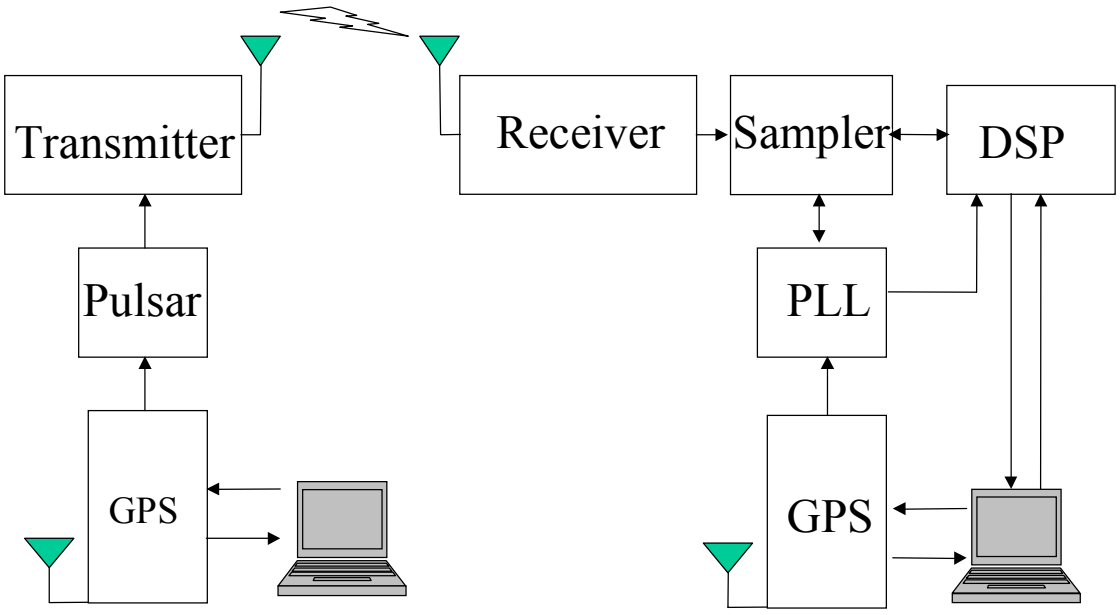

Figure 2.3 SSTDSP system block diagram

computer software to produce the power delay profile and other channel parameters

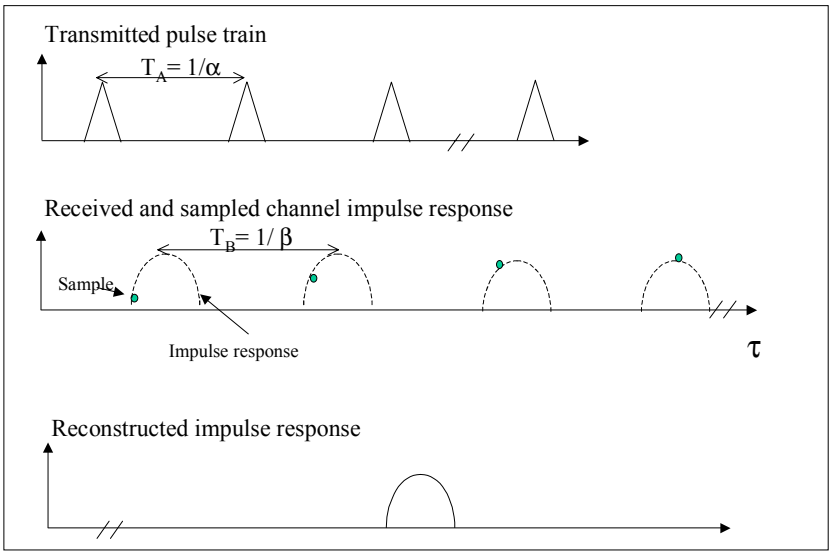

Figure 2.4 Transmit pulses and received channel response

including mean excess delay, RMS delay spread, and coherence bandwidth.

2.4 Studies Related to Characterizing LMDS Channels

Only a few sounding studies have been were done to characterize LMDS channels. The methods and results of these studies are described in this section.

A ray-tracing propagation simulation model was used in a study conducted by Anderson [18] to investigate the disperse nature of the transmission channel in a typical urban environment. RMS delay spread and coherence bandwidth were measured in the urban environment of downtown Eugene, Oregon. A study route was devised along one street and a ray-tracing study was carried out at points spaced every 5 meters along the route. The channel characteristics of dispersion were investigated in LOS and NLOS. The results showed that the degree of channel

dispersion varies widely from one location to another. Highly directional antennas could reduce channel dispersion. Depending on data rate and modulation type, high-speed transmission should be possible without equalizers, even if not LOS.

In the study conducted by Maurer, Didascalou, Engels, and Wiesbeck [19], 74 different propagation scenarios were investigated. These 74 locations were classified into free Fresnel zone (FFZ), obstructed Fresnel zone (OFZ), obstructed line of sight (OLOS) and non-line of sight (NLOS). A commercial LMDS system, Marconi Digital Multipoint System with 2 base stations and 9 terminals, was used to perform the measurements. Delay spread and coherence bandwidth were calculated based on the measured power delay profiles. For all measurement the mean value of delay spread was 158.54 ns. The delay spread was zero for most of the LOS/OLOS measurements. The maximum value was 157 ns, and the mean value was 13.34 ns. For NLOS, the delay spread increased drastically: it could reach even 1000ns. The mean value of standard deviation of delay for the NLOS channels was 443.19 ns. The histogram of the reflection delay spread was surprisingly small, according to the researchers. They concluded that this meant in some cases data transmission could be possible via a strong reflection path. The researchers also pointed out that vertical polarization is desirable for LMDS systems since for horizontal polarization, relative multipath power was increased, thus yielding a larger delay spread.

Ravi and Soma [20] investigated a model of an LMDS channel. In their study, some preliminary results of the propagation measurements conducted at 27.4 GHz in Singapore to obtain the characteristics of LMDS were described. Using

swept time delay cross-correlation (STDCC) the wideband impulse response was measured. The parameters include average excess delay and RMS delay spread. It was found that for distances greater than 0.5 km the excess path loss ranges from 25-60dB and was highly dependant on the nature of blockage. Four categories of blockage could be identified which are: LOS, near LOS, blocked by a single block and/or foliaged trees, and completely blocked by multiple blocks. The researchers concluded that the excess loss depended highly on the nature of blockage, and LOS or near LOS links were required for a satisfactory operation of LMDS. The delay profile showed that the RMS delay spread of 200 ns to 250 ns was quite common in this environment.

In Papazian, Hufford, Achatz, and Hoffman's study [21] narrowband CW signal and a 30.3 GHz wideband signal through a common traveling wave tube amplifier were used in the measurements. On the receiver side, a sliding correlator was used. Two survey sites were in Colorado and California. K-factor and delay spread were used to analyze the data collected. The results showed that the major source of attenuation in the channel was obstruction of the radio path by buildings and vegetation.

Continuous wave carrier carried out measurement of the LMDS channel was used by Chavero, Polo, Ramos, and Marti [22]. Direct LOS and non-LOS were surveyed on a university campus. The radio channel was statistically modeled using the Smirnov-Kolmogorov test to determine which radio propagation model best fits the experimental data. The link availability was derived from this model

using the cumulative distribution. Results showed serious influence of vegetation on attenuation.

Briso-Rodriguez, Vazquez-Castro, and Alonso-Montes [23] did a study on LMDS channel modeling of a wide-band measurement in an urban environment in Madrid, Spain. Four different sectors in Madrid were classified based on building height and density. The environments were measured using a time domain sliding correlator channel sounder. The bandwidth of the sounder measurement was 50 MHz. The transmitter was located in high buildings or towers and the receiver was moved in an area from 500 m to 5 Km away from the transmitter. All the measurements were taken in LOS. These measurements were processed to compute excess path loss, mean delay, RMS delay spread, and correlation bandwidth. The results showed that in a high business building area there was a very high excess path loss, 10 to 60 dB. The other three areas had lower and similar excess path loss, in the range of 3 to 12 dB. In historical and shopping center areas, the delay spread was the lowest, 50 to 60 ns. In an old building residential area, the delay spread ranged from 150 to 300 ns.

2.5 Conclusion

Based on the measurement done in the literature review, a table of LMDS channel parameters related to these studies above is summarized in Table 1. In the current study the sampling swept time delay short pulse (SSTDSP) sounder was used to characterize the channel response. Although the sounder has the capability to measure several parameters, the power delay profile was the focus of this study. The

power delay profiles collected in different measurement settings were to study the scattering phenomena on limestone wall and brick wall at 28 GHz.

Table 2.1 Summary of Results in the Literature

Study #	Frequency Band	Measurement	Delay Spread	Coherence Bandwidth	Location	Researcher
1	28 GHz	Ray-Tracing model	160 ns at30 m distance	0.5 MHz at 30 m	Urban area	Anderson (1999)
2	26 GHz	Marconi Digital Multipoint Systems	13.34 ns (mean)	6.3 MHz (mean of total locations)	LOS/OLOS	Maurer et al. (2000)
			443.19 ns (mean of SD)		NLOS	
3	27.4 GHz	Swept Time Delay Cross-Corelation	200 ns to 250 ns		LOS/NLOS	Ravi and Soma (1999)
4	30.3 GHz	Wideband signal & traveling wave tube amplifier	0 to 15.3 ns (122m to 419 m)		LOS/NLOS	Papazian et.al. (1997)
5	28 GHz	Time domain sliding corelator channel sounder	50 ns to 300 ns		LOS/Urban area	Briso-Rodriguez (2001)

Chapter 3 Measurement Procedures and Analysis

The purposes of these data collection measurements are to test the SSTDMP sounder and to study the scattering phenomena of limestone and brick walls in the 28 GHz LMDS band. This will lay the groundwork for other, more extensive, measurement campaigns. In the first step, the SSTDMP was used to take the power delay profile of the channel impulse response with the transmitter and receiver connected with a coaxial cable. The sounder system was then taken outdoors to be calibrated. Finally power delay profiles of channel impulse response were collected in different reflection settings on a limestone wall and a brick wall on the Virginia Tech Campus.

3.1 Calibration

The SSTDMP sounder is the first generation of this equipment and has never been used in field experiments before this study. In order to make sure that the sounder operated appropriately, we needed to conduct calibration procedures before using it to collect data for this study.

3.1.1 Impulse signal

A three-meter long coaxial cable was used to connect the transmitter output to the receiver input and the sounder board captured the impulse response of the channel and the data was collected. By using a coaxial cable rather than transmitting the signal through the air to the receiver, we expect that the impulse signal received should be essentially the same as the signal existing inside of the transmitter and

displayed on the oscilloscope. The result was exactly what we expected. The pulse was graphed in Figure 3.1.

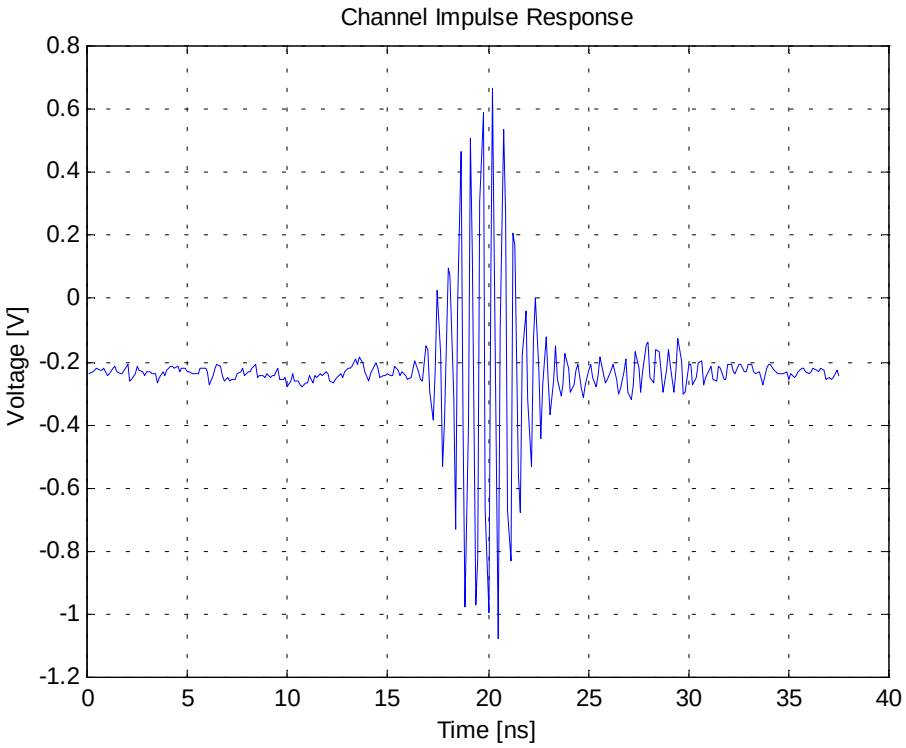

Figure 3.1 Channel impulse response obtained by the SSTDMP when connected to the transmitter by a coaxial cable.

3.1.2 Outdoor calibration measurement

To make sure the SSTDSP would take the measurement accurately, a calibration measurement was conducted. A 1.2-meter by 1.2-meter sheet of cardboard was covered with aluminum foil (Figure 3.2) to be used in calibration testing. Since the surface of the foil cardboard is relatively smooth, the board is expected to be a perfect reflector. Therefore, if the transmitter and receiver are

Figure 3.2 Calibration reflector

aimed to the reflection point on the reflector, the impulse signal reflected from the board and then received at the receiver should have the same waveform, but different signal strength, as the LOS signal. The reflected pulse should also arrive with a delayed time from the LOS pulse. To verify this assumption, the aluminum reflector was placed in open space, and the sounder system was positioned in several different distance settings from the reflector. The distance and incident angle set-ups are listed in Table 3.1, where *d1* is the distance from the transmitter to the reflector, *d2*, the distance from the receiver to the reflector, and *dLOS* is the direct path between transmitter and receiver.

Table 3.1 Calibration Measurement Set-ups

Incident Angle	**d1**		**d2**		**dLOS**		diff	diff-delay
[deg]	[m]	[ft]	[m]	[ft]	[m]	[ft]	[m]	[ns]
15	9	29.0	9	29.0	4.6	15.0	13.1	43.7
22.5	6	19.6	6	19.6	4.6	15.0	7.4	24.6
30	5	15.0	5	15.0	4.6	15	4.6	15.3

The measurement results showed that there were two impulses received when the transmitter and receiver antenna were vertically polarized and aimed toward the reflector. The first pulse was the LOS pulse and the second pulse was the reflected pulse. The reflected pulse arrived later than the LOS pulse and the reflected pulse had a similar waveform as the LOS pulse but different signal strength. Examples of the LOS pulse and reflected pulse data collected are given in Figures 3.3. LOS pulses may have smaller amplitude. This is because the transmitter and the receiver were aiming toward the reflector. The LOS signal was in the side lobe of the antenna beam, therefore it had a smaller voltage amplitude than the reflected pulse.

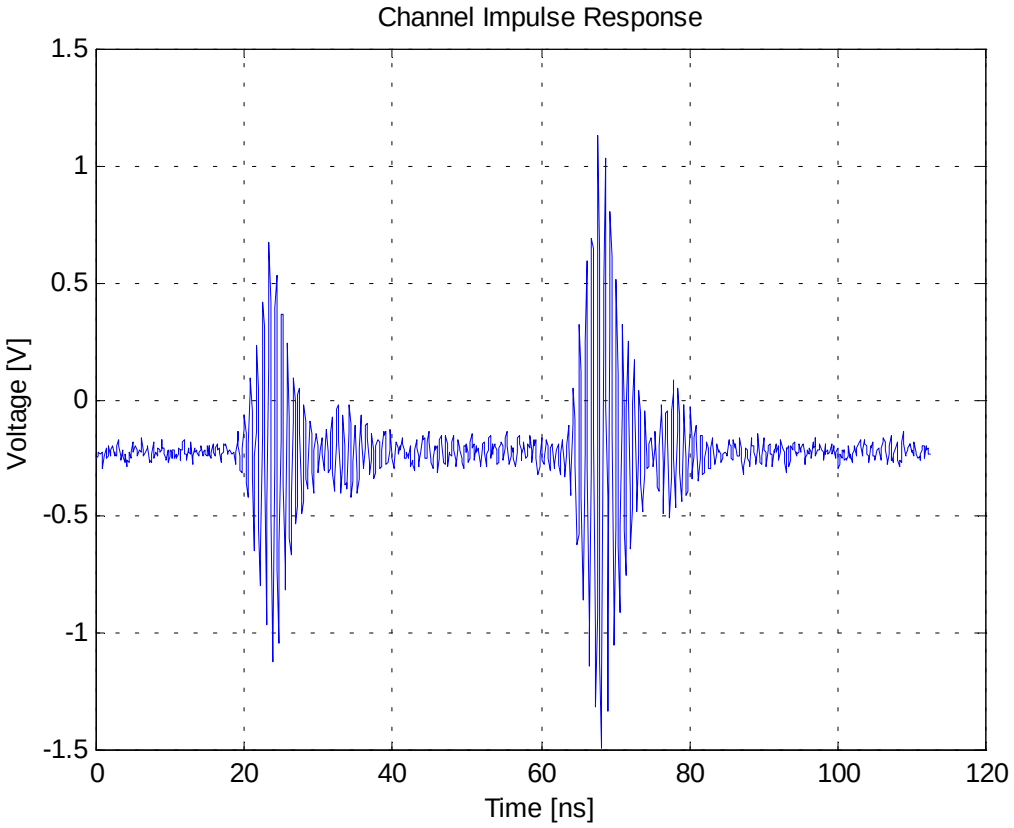

Figure 3.3 LOS pulse and reflected pulse (TX/RX to Reflector = 8.8m)

3.1.3 Antenna pattern measurement

The LMDS radio used in the SSTDSP sounder is a Motorola Spectra Point radio which has a 90° antenna. Since we were not able to get the detailed specification of the antenna pattern, we did an outdoor field measurement to estimate the antenna pattern. This antenna pattern was used for data analysis of calibration data and field data in Chapter 4.

To measure the antenna pattern, the transmitter was connected with an HP8648C signal generator, which sent out one tone signal at 1850 MHz with 0 dBm power and up converted by the transmitter to the LMDS band. The receiver was connected with a HP8594E spectrum analyzer to measure the received power. The receiver and transmitter were placed 10 meters away from each other. The receiver was stationary, but the transmitter was rotated in 15° increments from the direct path (Figure 3.4).

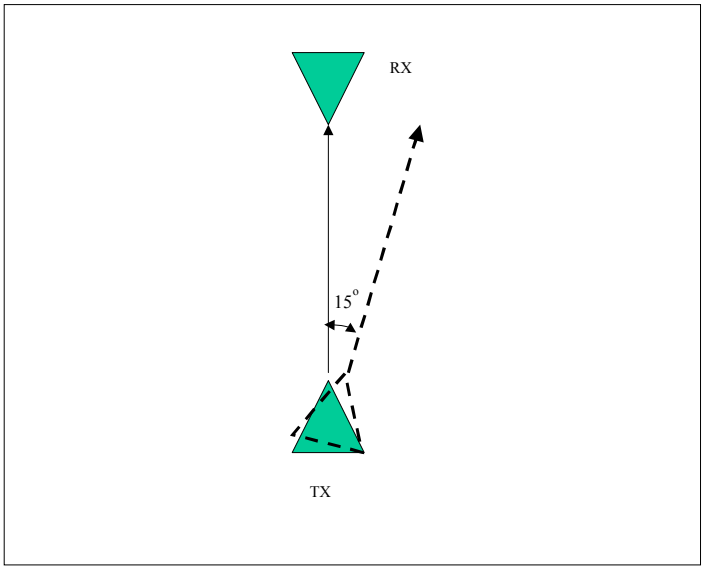

Figure 3.4 Antenna pattern measurement set-up

Altogether there were 24 data points for the antenna gain. Using these data points, a 90° perpendicular polarization (antenna is vertically polarized) relative antenna gain was estimated and plotted with Matlab. Figure 3.5 shows the estimated antenna pattern.

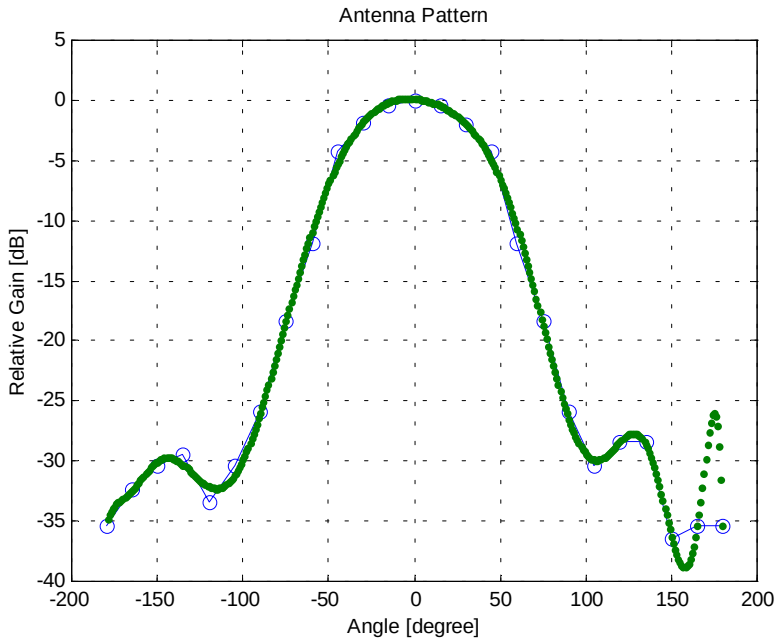

Figure 3.5 Antenna pattern

3.1.4 Calibration data analysis

In Section 3.1.2 we described how we carried out the calibration measurements. After we measured the antenna pattern, we also analyzed the calibration data for the three set-ups described in Table 3.1. From the raw data file for each set-up, we identified the maximum power measured for the reflected pulse and LOS pulse. Then using the ratio of the measured power of reflected pulse and

LOS pulse, as well as equations 1.12 and 1.19, we were able to estimate the cross-section area for each incident angle set-up:

$$\frac{(P_R)_{ref}}{(P_R)_{LOS}} = \frac{P_t G_t G_r A\lambda^2 / (4\pi)^3 (d_t d_r)^2}{P_t G_{t(\theta)} G_{r(\theta)} \lambda^2 / (4\pi)^2 (d_{LOS})^2} \tag{3.1}$$

From Equation 3.1, measured cross-section area *A* can be derived as:

$$A = \frac{(P_R)_{ref} \cdot 4\pi (d_t d_r)^2 G_{t(\theta)} G_{r(\theta)}}{(P_R)_{LOS} \cdot d_{LOS}} \tag{3.2}$$

This measured cross-section area was compared with the physical area of the aluminum reflector multiplied by the cosine of the incident angle. Table 3.2 summarizes the results, where angle is the incident angle, *d1* is the distance to the

Table 3.2 Calibration Data

Angle [degree]	d1 [m]	d2 [m]	dLOS [m]	GainTX	GainRX	Plos	Pspec	A measured [m*m]	A*Cos(Angle) [m*m]
15	8.8	8.8	4.6	0.0134	0.0134	0.8062	1.8403	1.460	1.436
22.5	6	6	4.6	0.0332	0.0332	1.3116	0.8082	0.523	1.37
30	5	5	4.6	0.0854	0.0854	2.5871	5.185	5.425	1.29

transmitter, *d2* is the distance to the receiver, *dLOS* is the direct path, *GainTX* is the transmitter antenna gain, *GainRX* is the receiver antenna gain, *Plos* is the power received through direct path, *Pspec* is the power received through the reflected pulse, *A measured* is the cross-section area A measured by equation 3.2 and *A*Cos(Angle)* is the aluminum reflector area multiplied by the cosine of the incident angle.

The measured cross-section area is equivalent to the physical area multiplied the cosine of the incident angle for 15^o but not for 22.5^o and 30^o. This may be due to the wind bending the reflector and affecting the measurement.

3.2 Reflection/Scattering Measurements on Two Kinds of Walls

To better understand the rough surface scattering phenomena, the reflection data from two different kinds of walls, limestone and brick, were studied with the

Figure 3.6 Limestone wall (top) and brick wall (bottom) used in the study

SSTDSP sounder at two locations on the Virginia Tech campus: the north side limestone wall on Hancock Hall and the north side brick wall on Lane Hall. Photos of these walls are shown in Figure 3.6.

3.2.1 Limestone wall measurement

The incident angle varied from 5 to 60 °s and the distance from the wall to the transmitters and receivers varied from 3 meter to 21 meters in the measurement set-ups (Table 3.3). The difference between the LOS pulse and reflected pulse arrival time (diff_del) ranged from 11.72 ns to 54.81 ns.

Table 3.3 Measurement Set-ups

Incident Angle	d1		d2		dLOS		diff_dis	Arrival Time Difference
[deg]	[m]	[ft]	[m]	[ft]	[m]	[ft]	[m]	[ns]
5	6.00	19.68	6.00	19.68	1.05	3.43	10.95	36.54
5	3.00	9.84	9.00	29.53	6.07	19.91	5.93	19.79
5	9.00	29.53	3.00	9.84	6.07	19.91	5.93	19.79
5	9.00	29.53	9.00	29.53	1.57	5.15	16.43	54.81
10	6.00	19.68	6.00	19.68	2.08	6.84	9.92	33.08
10	3.00	9.84	9.00	29.53	6.27	20.56	5.73	19.13
10	9.00	29.53	3.00	9.84	6.27	20.56	5.73	19.13
10	9.00	29.53	9.00	29.53	3.13	10.25	14.87	49.61
15	6.00	19.68	6.00	19.68	3.11	10.19	8.89	29.67
15	3.00	9.84	9.00	29.53	6.58	21.57	5.42	18.09
15	9.00	29.53	3.00	9.84	6.58	21.57	5.42	18.09
15	9.00	29.53	9.00	29.53	4.66	15.28	13.34	44.50
30	6.00	19.68	6.00	19.68	6.00	19.68	6.00	20.01
30	3.00	9.84	9.00	29.53	7.94	26.04	4.06	13.55
30	9.00	29.53	3.00	9.84	7.94	26.04	4.06	13.55
30	9.00	29.53	9.00	29.53	9.00	29.53	9.00	30.02
45	6.00	19.68	6.00	19.68	8.49	27.84	3.51	11.72
45	6.00	19.68	9.00	29.53	10.82	35.49	4.18	13.95
45	9.00	29.53	6.00	19.68	10.82	35.49	4.18	13.95
45	9.00	29.53	9.00	29.53	12.73	41.76	5.27	17.59
60	15.00	49.21	15.00	49.21	25.98	85.24	4.02	13.41
60	15.00	49.21	18.00	59.05	28.62	93.89	4.38	14.62
60	18.00	59.05	15.00	49.21	28.62	93.89	4.38	14.62
60	21.00	68.90	21.00	68.90	36.37	119.33	5.63	18.77

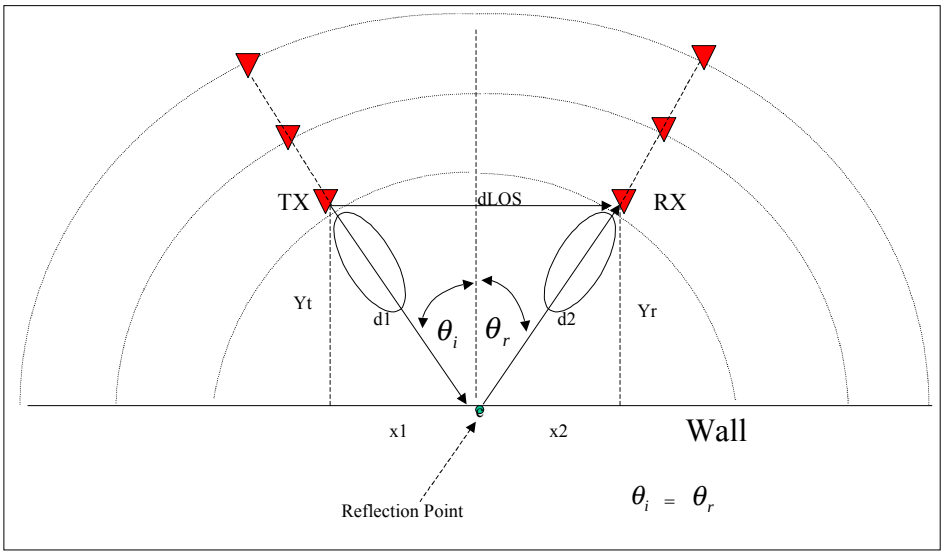

Figure 3.7 Measurement set-up

Before placing the transmitter and receiver at the planned positions, a measuring tape, string and surveying flags were used to mark the positions (Figure 3.7).

3.2.2 Brick wall measurement

Similar set-ups to collect data in brick wall location were used. The incident angle and distance from the wall were all the same as limestone wall data collection.

3.3 Conclusion

The calibration and field data collection took about two months. Altogether more than 240 power delay profile files of data were collected. The data used for analysis were collected in 4 different days—two days for limestone and two days for brick walls. We draw conclusions from the power delay profiles and discuss in Chapters 4 and 5.

Chapter 4 Results

In this chapter we describe the procedure used in processing the data collected and report the results. The data collected based on the measurement set-up description given in Chapter 3 were saved. For each measurement sep-up, five delay profiles were taken. All together there were 250 files used for data processing, 240 files for wall measurements and 10 files for free space LOS reference pulses. In each delay profile, the raw data collected by the sounder were the voltage samples of the channel impulse response. Each data file consists of voltage data points and can be graphed with any software packages. Matlab program is used to graph the power delay profile for each measurement set-up in data processing.

4.1 Data Processing Procedures

Raw data for each file was first graphed as a voltage vs. time profile, as shown in Figure 4.1. Five delay profiles for each measurement set-up were compared to make sure that they were the same. Since they all looked the same, one was used to graph the power delay profile. The raw data was filtered with the Matlab code so that the absolute value of the voltage envelope could be traced (Figure 4.1).

Power was then calculated and graphed. An example can be found in Figure 4.2 Normalized power in dB was graphed for further analysis of the pulse width of the reflected pulse in each delay profile. The power delay profiles for limestone and brick reflected pulses for each set-up were used to analyze the scattering phenomena.

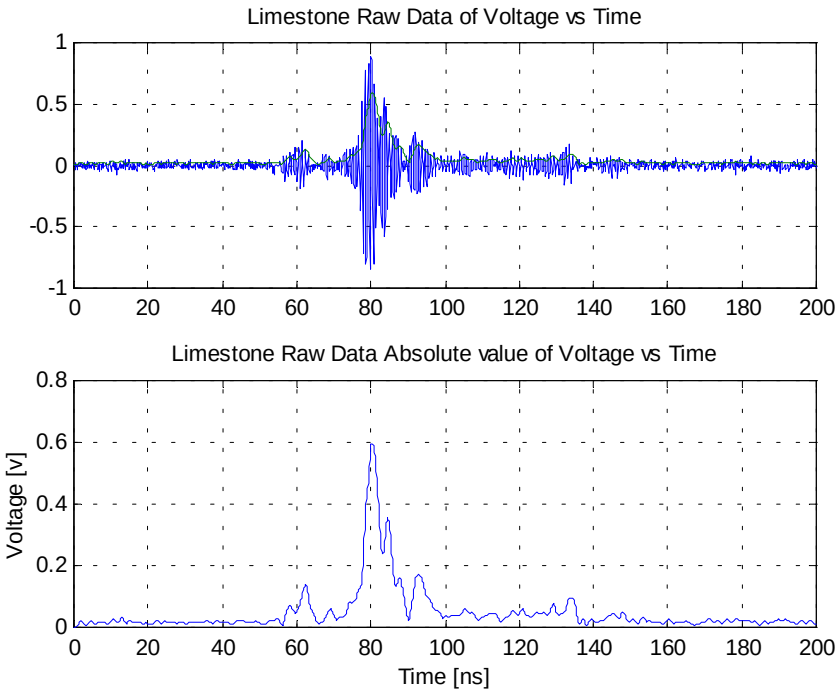

Figure 4.1 Raw data and envelope of the absolute value

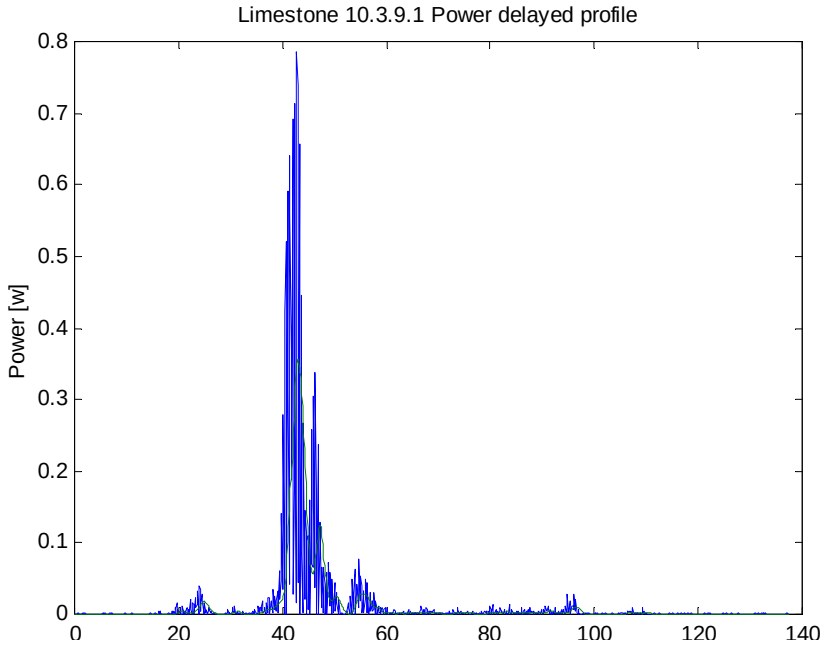

Figure 4.2 Power delay profile (10.3.9.1 represents: incident angle =10° , d1 = 3 m, d2 = 9 m and 1 = the first file of five raw data files of this particular set-up.)

Altogether there were 25 profiles used for data analysis: one of two free space LOS pulses with transmitter and receiver antenna facing each other, as well as 24 profiles of limestone and brick wall set-ups. One of these examples can be found in Figure 4.3.

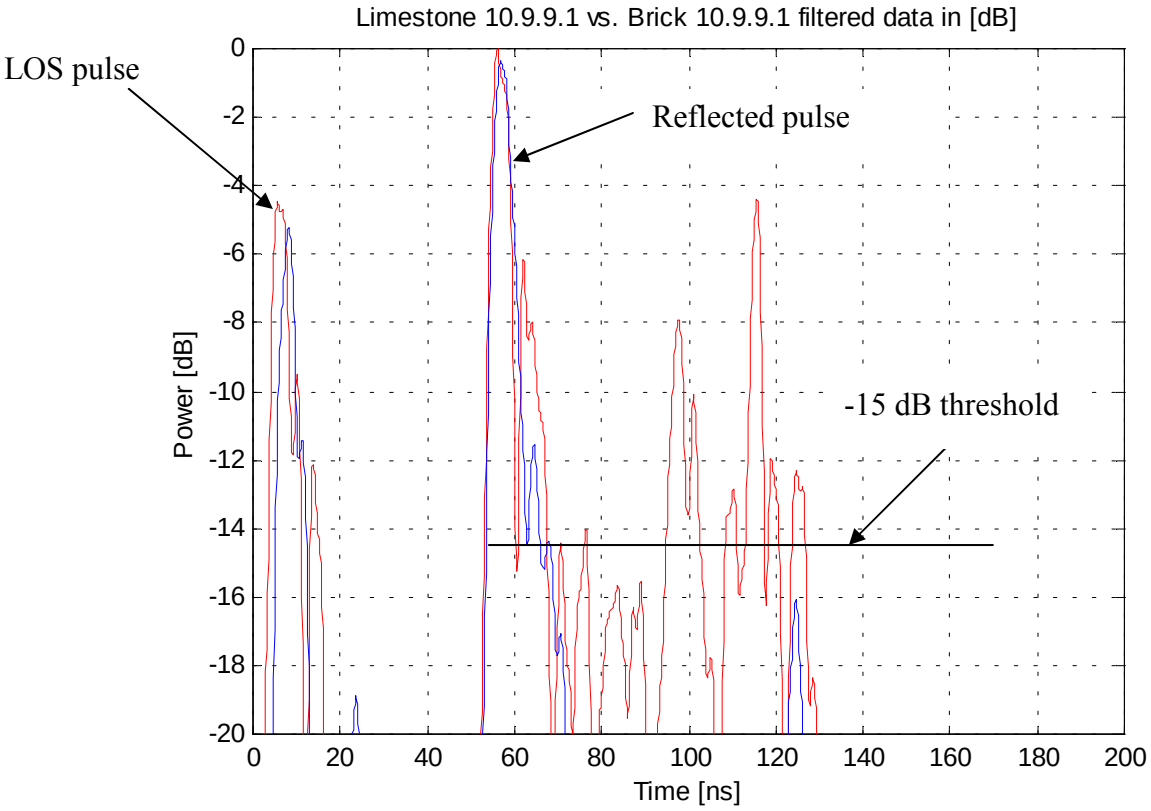

Figure 4.3 Comparison of limestone/ brick power delay profiles (Limestone pulses are shown in red. Brick is shown in blue.)

For each profile, the pulse width of the reflected pulse at -3 dB and -10 dB points, and the maximum excess delay spread at –15 dB threshold were estimated and recorded. The maximum excess delay is the time delay spread of the energy of the measured multipath component falls 15 dB below the peak value of the reflected pulse. Table 4.1 shows the raw data of all of the reflected pulse widths, maximum

excess delays and "excess pulse duration" which is the reflection pulse width less the free space LOS reference. LOS reference pulse widths are 3 ns at –3 dB and 7.5 ns at –10 dB power levels.

Table 4.1 Summary of Raw Data

				Limestone					Brick				
				Reflected Pulse Width		Excess Delay	Excess Pulse Duration		Reflected Pulse Width		Excess Delay	Excess Pulse Duration	
Case #	Incident Angle	d1	d2	3 dB	10 dB	15dB	3dB	10dB	3 dB	10 dB	15dB	3 dB	10 dB
	[deg]	[m]	[m]	[ns]	[ns]		[ns]	[ns]	[ns]	[ns]		[ns]	[ns]
1	5	6	6	2	3	72	-1	-4.5	4	8.5	18.5	1	1
2	5	3	9	2.5	5	16	-0.5	-2.5	2.5	5	20	-0.5	-2.5
3	5	9	3	4.5	8.1	10	1.5	0.6	4.5	8.1	18	1.5	0.6
4	5	9	9	8	13	85	5	5.5	6	11	18	3	3.5
5	10	6	6	4	9	70	1	1.5	4.5	9	18	1.5	1.5
6	10	3	9	3	8	19	0	0.5	4.5	10	17	1.5	2.5
7	10	9	3	4	7.5	15	1	0	2	8	15	-1	0.5
8	10	9	9	4	6	77.5	1	-1.5	4	8	15	1	0.5
9	15	6	6	4	9	48	1	1.5	4	11	19	1	3.5
10	15	3	9	5	10	18	2	2.5	5	6	18	2	-1.5
11	15	9	3	3	5	16	0	-2.5	2.5	6.5	9	-0.5	-1
12	15	9	9	4	11	76	1	3.5	3.5	6	12	0.5	-1.5
13	30	6	6	4	11	18	1	3.5	4	8	12	1	0.5
14	30	3	9	3	9	24	0	1.5	4	6	16	1	-1.5
15	30	9	3	6	9	17	3	1.5	4	8	16	1	0.5
16	30	9	9	4	10	45	1	2.5	4	7	13	1	-0.5
17	45	6	6	6	8	26	3	0.5	3.5	10	18	0.5	2.5
18	45	6	9	4	5	32	1	-2.5	3.5	10	18	0.5	2.5
19	45	9	6	2	4	30	-1	-3.5	4.5	11	18	1.5	3.5
20	45	9	9	8	10	17	5	2.5	7.5	10	18	4.5	2.5
21	60	15	15	3.5	8	24	0.5	0.5	4	8	12	1	0.5
22	60	15	18	3	9	24	0	1.5	3.5	9	16	0.5	1.5
23	60	18	15	4	9	31	1	1.5	3.5	9	10	0.5	1.5
24	60	21	21	4	8.5	23	1	1	3.5	8	12	0.5	0.5
			Mean	4.1	8.1	34.7	1.1	0.6	4.0	8.4	15.7	1.0	0.9
			SD	1.5	2.4	23.5	1.5	2.4	1.1	1.7	3.1	1.1	1.7

4.2 Analysis of Power Delay Profile Raw Data: Scattering

Based on the raw data of the reflected pulse width in Table 4.1, a Microsoft Excel program was used to plot some graphs. Conclusions of the scattering phenomena of the limestone wall and brick wall were found and are listed below

1) Limestone and brick walls do not exhibit significant diffuse scattering. Compared to the LOS reference pulse width the reflected pulse width at -3 dB and at -10 dB are not significantly different. The excess delay duration represents this difference. For all measurement set-ups, the mean value of the excess pulse duration at -3 dB is 1.1 ns for limestone and 1 ns for brick; 0.6 ns for limestone and 0.9 ns for brick at –10 dB power level. Figure 4.4 shows the reference LOS pulse power profile and Figure 4.5 and Figure 4.6 show the average value of the excess pulse duration for each incident angle measurement set-up.

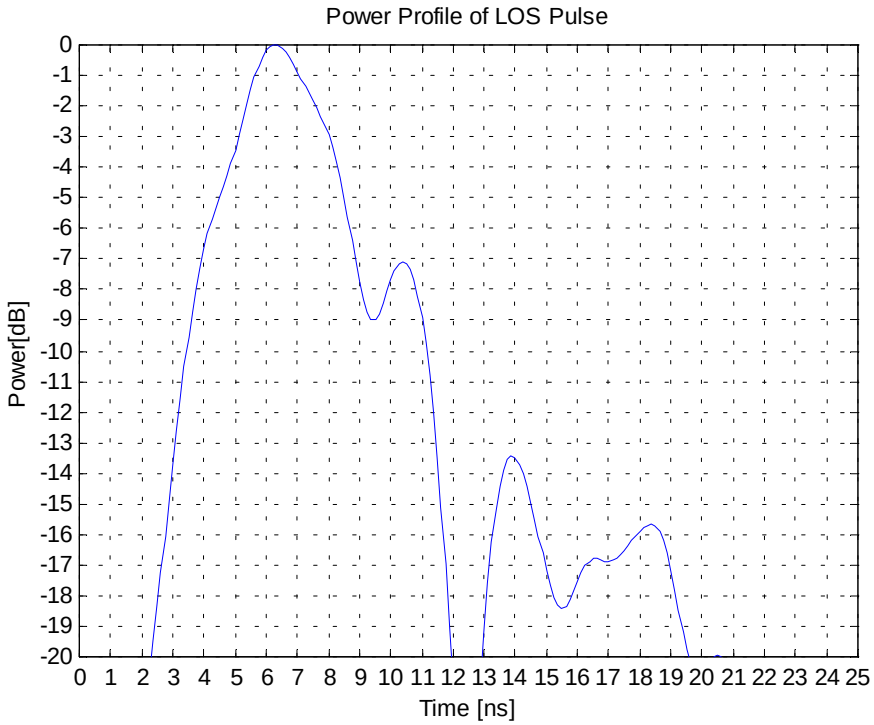

Figure 4.4 LOS pulse power profile

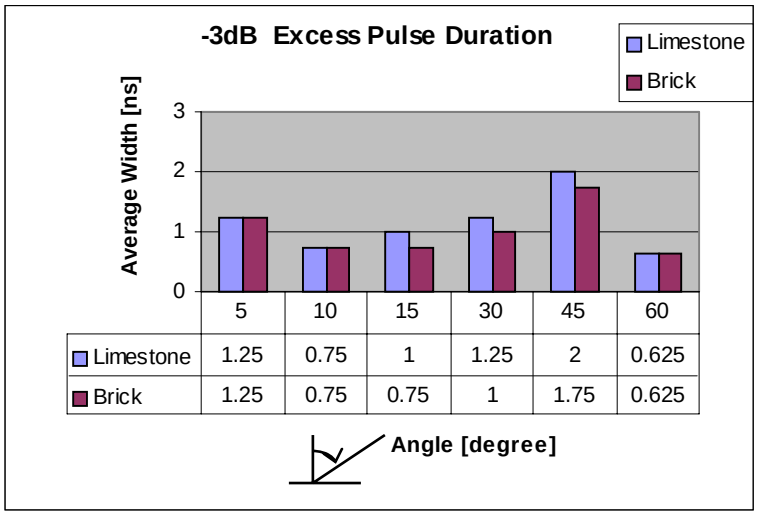

Figure 4.5 Average excess pulse duration (-3 dB)

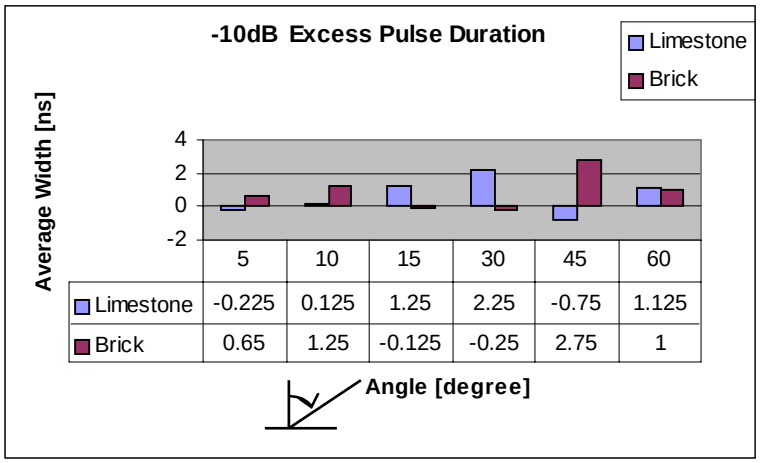

Figure 4.6 Average excess pulse duration(-10 dB)

2) The limestone wall seemed to show more energy spread than the brick wall. The values of the reflected pulse excess delay at –15 dB for limestone wall for 21 out of 24 measurement set-ups are larger than those for the brick wall. The limestone mean value of excess delay is 34.7 ns and 15.7 ns for brick. The results can be found in the Figure 4.7.

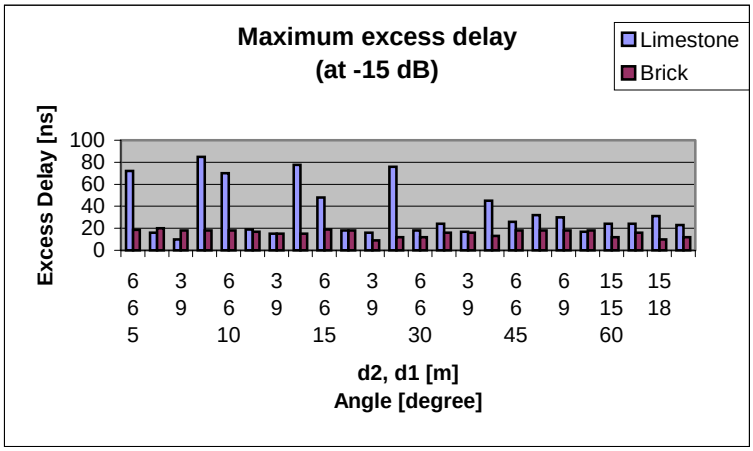

Figure4.7 Maximum excess delay at –15 dB

3) With equal transmitter (d1) and receiver (d2) distances to the limestone wall, the 9 meter setups exhibit larger maximum excess delay at –15 dB than those at 6 meter setups. Also as the incident angle increases from 5° to 45°, the excess

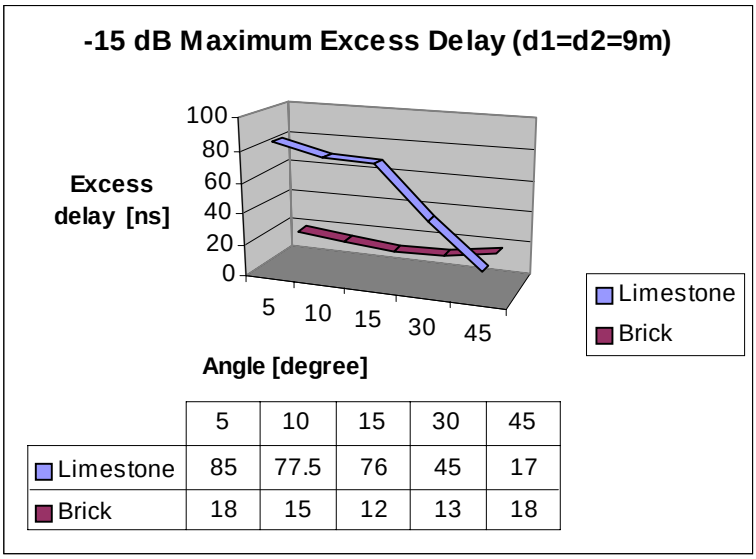

	5	10	15	30	45
Limestone	85	77.5	76	45	17
Brick	18	15	12	13	18

Figure 4.8 Excess delay for equal distance set-up (9m)

delay decreases. However, the brick wall does not show any of these trends. Figure 4.8 and Figure 4.9 show the results.

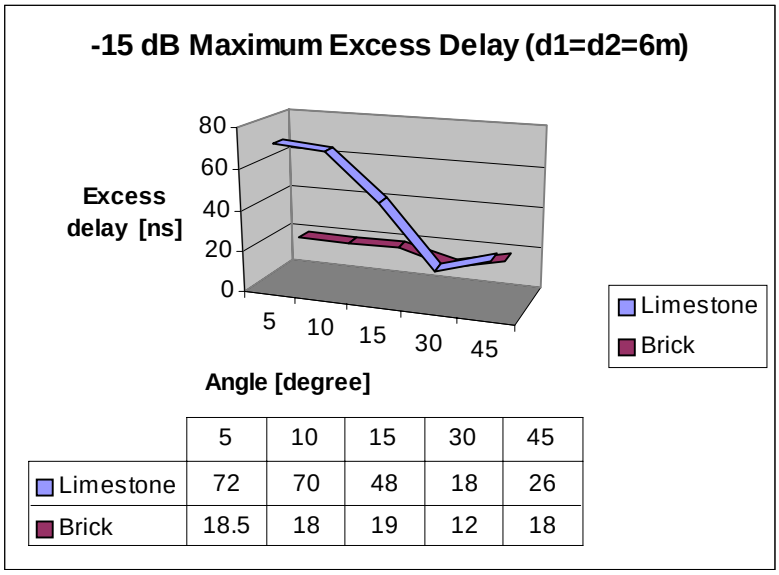

	5	10	15	30	45
Limestone	72	70	48	18	26
Brick	18.5	18	19	12	18

Figure 4.9 Excess delay for equal distance set-up (6 m)

4). When the receiver distance (d2) is greater than the transmitter distance (d1) to the wall, the maximum excess delay is larger for 5° to 45° angle set ups. The excess delays for d1=3 m and d2 = 9 m set ups exceed d1 = 9 m and d2 =3 m set-ups when incident angle ranges from 5° to 30°. The same is true for the 45° set-up when d1 = 6 m and d2 = 9 m. Figure 4.10 shows the comparison of results for the limestone wall and Figure 4.11 shows the comparison for the brick wall.

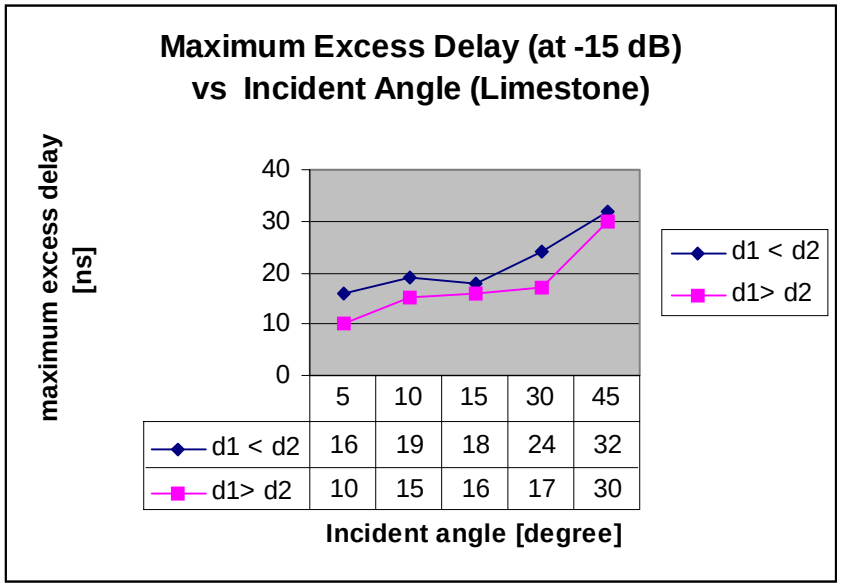

Figure 4.10 Maximum excess delay and incident angle comparison (limestone)

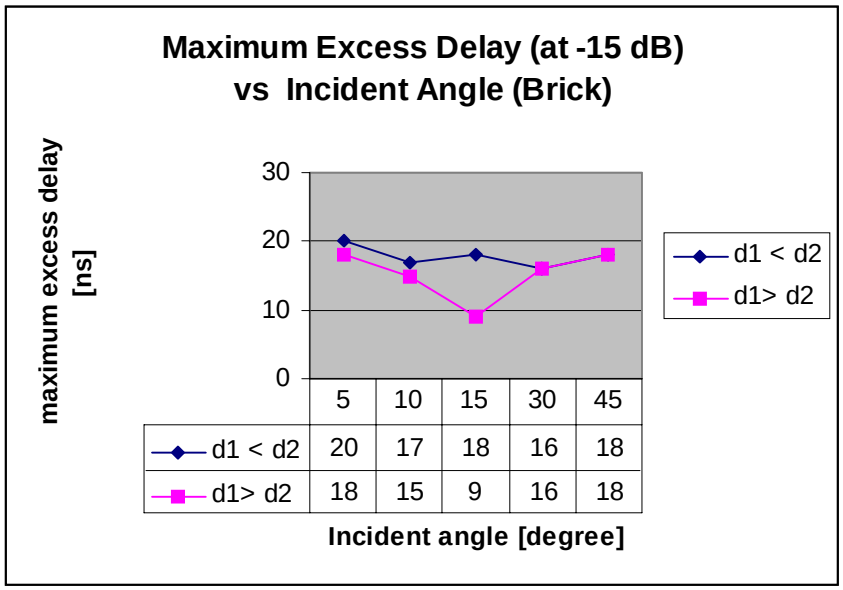

Figure 4.11 Maximum excess delay and incident angle comparison (brick)

4.3 Analysis of Reflection Coefficients

From the raw data collected we have approximated the reflection coefficient for each incident angle set-up by using the following equation:

$$|\Gamma| = \frac{V_s}{V_{LOS}} \sqrt{g(\theta_{TX}) \cdot g(\theta_{RX})} \cdot \frac{(d_1 + d_2)}{d_{LOS}} \tag{4.1}$$

where V_s is the maximum absolute voltage value of the spectra reflection pulse and V_{LOS} is the maximum absolute voltage value of the LOS pulse. d_1, d_2 and d_{LOS} represent the distances from the transmitter and receiver to the wall and LOS distance for each measurement set-up, respectively. Section 3.2, Table 3.2 and Figure 3.5 have all the detailed description of the measurement set-ups. $g(\theta_{TX})$ and $g(\theta_{RX})$ are the antenna gains of the transmitter and receiver for each power delay profile incident angle set-up. These antenna gains were based on the antenna pattern measurement describe in Chapter 3. Equation 4.1 is equivalent to equation 1.22 in Chapter 1 but with antenna gain taken into account.

The reflection coefficients were calculated for the limestone and brick walls. The results are shown in Table 4.2. As the incident angle gets bigger, the reflection coefficient seems to increase for both kinds of wall. Figure 4.12 and Figure 4.13 show the data points of reflection coefficient corresponding to each incident angle with different distance set-ups for each kind of wall.

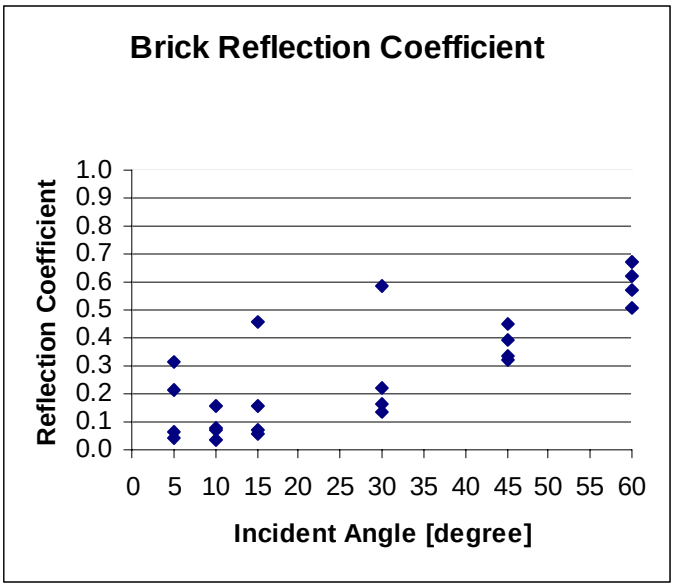

Figure 4.12 Brick reflection coefficient (perpendicularly polarized)

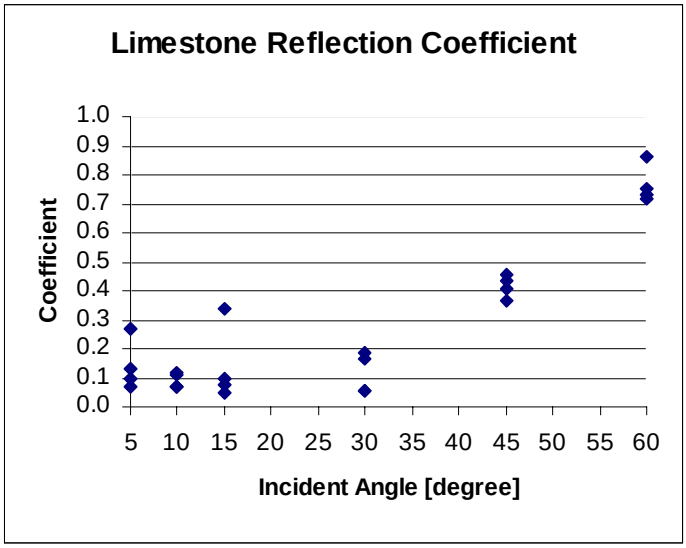

Figure 4.13 Limestone reflection coefficient (perpendicularly polarized)

Table 4.2 Reflection Coefficients

					Reflection Coefficient	
Case #	Incident Angle	d1	d2	dLOS	Brick	Limestone
	[deg]	[m]	[m]	[m]		
1	5	6	6	1.0	0.042	0.100
2	5	3	9	6.1	0.212	0.133
3	5	9	3	6.1	0.311	0.269
4	5	9	9	1.6	0.066	0.072
5	10	6	6	2.1	0.076	0.067
6	10	3	9	6.3	0.157	0.117
7	10	9	3	6.3	0.036	0.112
8	10	9	9	3.1	0.070	0.068
9	15	6	6	3.1	0.054	0.050
10	15	3	9	6.6	0.455	0.339
11	15	9	3	6.6	0.155	0.100
12	15	9	9	4.7	0.074	0.074
13	30	6	6	6.0	0.587	0.184
14	30	3	9	7.9	0.136	0.055
15	30	9	3	7.9	0.162	0.056
16	30	9	9	9.0	0.223	0.164
17	45	6	6	8.5	0.392	0.433
18	45	6	9	10.8	0.324	0.406
19	45	9	6	10.8	0.335	0.364
20	45	9	9	12.7	0.451	0.456
21	60	15	15	26.0	0.507	0.730
22	60	15	18	28.6	0.622	0.860
23	60	18	15	28.6	0.569	0.750
24	60	21	21	36.4	0.671	0.720

Chapter 5 Discussion

In this chapter, we discuss the results of the data analysis, describe the equipment, describe the contribution and make suggestions for future research.

5.1 Scattering Phenomena

Although most of the power delay profiles look quite reasonable for analysis, the data from the 45° and 60° set-ups on limestone are quite difficult to interpret. This is because the LOS pulse and reflected pulse are not separated far enough in time. If the location for measurement has a big enough open space and not many obstructions, this will not be a problem, since we can have longer distance to set up the equipment to collect data that have clear separation between the LOS pulse and reflected pulse. However, the locations for data collection on Virginia Tech campus are quite limited and sufficient open space is not easily found.

At the 28 GHz LMDS band, the diffuse scattering phenomena are not as evident as we had expected, since in most of the set-ups the reflected pulse width at -3 dB and -10 dB power levels are not that much different from the LOS pulse width. However there are two profiles that have more than 4 ns excess pulse duration at –3dB level: Limestone 5° and 45° incident angle at d1 = 9 m and d2 =9 m set-ups. It is possible that for very small angles, diffuse scattering does exist for rough surfaces. Further studies might be needed. For 45°, it is possible that the difficulties of interpretation of the power delay profile contribute to the error of interpreting the pulse width.

The fact that the limestone wall is rougher than the brick wall may explain why the limestone wall has wider excess delay spread at –15 dB than those from the brick wall. When the transmitter and receiver are located the same distance from the wall, the longer distance seems to result in more excess delay at –15 dB. The same situation happens when the receiver distance to the wall is greater than the transmitter distance from the wall. The reasons contributing to this phenomenon may be that when receiver is farther away from the wall, more energy is spread out leaving more opportunity for multi-path propagation. Therefore, the excess delay may increase.

5.2 Reflection Coefficient

In Section 1.4, we reviewed several studies related to rough surface reflection coefficient measurement. In the study of Landron et al. [12], reflection coefficients at 1.9 GHz and 4 GHz were derived from the theoretical perspective and the measured data; in the study of Kim et. al. [14], reflection coefficients at 28 GHz were measured. The results of our calculation of reflection coefficients seem to be consistent with the findings of Landron et al., and Kim et al. As the incident angle increases, the perpendicularly polarized reflection coefficient also increases. Table 5.1 shows the trends observed in previous research and the present study.

Table 5.1 Perpendicular reflection coefficient ($\Gamma_{\perp}$)

Wall	Incident angle	Present study (28 GHz)	Landron et. al. (4 GHz)	Kim et.al.(28GHz)
Limestone	0		~0.1 to 0.5	
	5	~ 0.1		
	10	~ 0.1		
	15	~ 0.1	~ 0.1 to 0.3	
	30	~ 0.2	~0.2 to 0.6	
	45	~ 0.4	~ 0.15 to 0.35	
	60	~ 0.7	~0.1 to 0.25	
Brick	0		~0.35	
	5	~ 0.1		
	10	~ 0.1		
	15	~0.1	~ 0.4	
	30	~ 0.2	~0.35	
	45	~ 0.4	~0.35	
	60	~ 0.6	~0.75	
Cement	5			~ 0.1
	10			~ 0.1
	15			~ 0.08
	30			~ 0.15
	45			~ 0.17
	60			~ 0.35
	70			~ 0.5

5.3 The SSTMDP Sounder

The sounder equipment used in this study is in its first generation. As mentioned in the data collection chapter, it took about two months to collect data. The main reason was that the equipment broke down often when it was taken out to do the field measurements. Since the sounder is composed of many modules, it is often time consuming to figure out which component has the problem. Most of the reasons contributing to the equipment breaking down were related to the power supply connection or cable connection getting loose while the sounder was being moved out to the field. Therefore for future applications, it will be necessary to have

a better package of the whole system so the equipment can be transported easily for field study.

5.4 Summary of Contributions

As indicated in Section 5.1 and Section 5.2, this present study has identified that diffuse scattering exists in the 28 GHz LMDS band for limestone and brick walls. This scattering phenomenon has not been found in such a detailed manner in previous studies reported in the literature. We have also found that the perpendicular reflection coefficient increases and the maximum excess delay decreases as the incident angle increases. The implication of this finding is that if reflectors are used in the shadowed area, the incident angle needs to be large.

5.5 Suggestions for Future Research

The LMDS radio used in this study has a relatively wide antenna beam (90°). For future study of scattering phenomena, one may consider using a smaller angle beam width to reduce the possibility of obstructions causing scattering within the beam width, which complicates interpretation of the reflected pulse width.

There are only two kinds of wall used in this study. Studying the scattering phenomena of glass walls may be significant since many buildings in city environments have large expanses of glass. It is also necessary to have the same distance set up for all angles, so it is easier to compare the data. The distance set-ups used in this study range from 3 meter to 21 meter, all being quite small compared to expected distances for operational systems in reality. Investigating longer distance

set-ups in the future to see whether the scattering phenomenon is the same is recommended for future study.

For further study, repeating the measurements in more locations to see whether this difference holds for all locations can be important. It is also recommended that all measurements at one location should be taken in one day so one can be sure that the equipment and measurement set-ups are in the same condition. This will help one avoid different conditions in the data collection process.

In chapter 1, it is mentioned that a number of studies suggesting that the reflection pulses may be used in non-LOS areas for the LMDS band. Since in this study we have found that reflected pulses have bigger amplitudes and less excess delay as the incident angle gets bigger, we have reason to believe that reflected signals can be used in non-LOS. To further prove this point, the sounder developed in this study should be applied to non-LOS areas to investigate how to aim the transmitter or receiver antennas to receive the useful reflected signal.

References

[1] Nordboten, A. LMDS Systems and Their Application. *IEEE Communications Magazine*, Vol. 38 No. 6, June 2000, pp. 150-154.

[2] DeCruyenaere, J. "Radio Coverage of Mill-Wave Broadband Wireless Access Systems in Suburban Area". Ph.D. Dissertation, Carleton University, Ottawa, Ontario, Canada, April, 2000.

[3] Rappaport, T. S. Wireless Communications: Principles and Practice (2nd Ed). Prentice Hall, NJ. 2002.

[4] Bacon, D. F. "Introduction to diffraction, reflection and scattering" in *Propagation of Radio Waves*, Edited by M. P. M. Hall, L. W. Barclay & M.T. Hewitt, 1996.

[5] Stutzman, W. L. *Polarization in Electromagnetic Systems, A*rtech House, Norwood, MA, 1993.

[6] Pratt, T. and Bostian, C. *Satellite Communication, John* Wiley & Sons, New York, 1986.

[7] Livingston, D. *The Physics of Microwave Propagation*, Prentice Hall, New Jersey, 1970.

[8] Boithias, L. *Radio Wave Propagation*, McGraw-Hill Inc., New York, 1987.

[9] Ament, W. S. Toward a Theory of Reflection by a Rough Surface. *Proceedings of the IRE*, Vol. 41, No. 1, January 1953, pp. 142-146.

[10] Skolink, I. M. *Introduction to Radar Systems*, McGraw-Hill Inc, Boston, 2001.

[11] Hayn, A., Rose, R. and Jakoby, R. Multipath Propagation and LOS Interference Studies for LMDS Architecture. *Eleventh International Conference on Antennas and Propagation.* (IEE Conf. Pub. No. 480). IEE Part vol. 2, 2001, pp. 686-90.

[12] Landron, O. Feuerstein, M. J., and Rappaport, T. S. In Situ Microwave Reflection Coefficient Measurements for Smooth and Rough Exterior Wall Surfaces. *IEEE Vehicular. Technology Conference*. Secaucus, NJ, May 18-20, 1993.

[13] Landron, O. Feuerstein, M. J., and Rappaport, T. S. A Comparison of Theoretical and Empirical Reflection Coefficients for Typical Exterior Wall Surfaces in a Mobile Radio Environment. *IEEE Transactions on Antennas and Propagation*, Vol. 44 No. 3, March 1996.

[14] Kim Y, Yang, K., and Kim, S. Scattering Characteristics of Surface Roughness in Frequency and Incident Angle Dependent at Millimeter-wave. *IEEE Microwave Conference*, Asia Pacific, 1999.

[15] Seidel, S. Y. and Arnold, H. W. Propagation Measurements at 28 GHz to Investigate the Performance of Local Multipoint Distribution Service (LMDS) *IEEE Global Telecommunications Conference*. IEEE Part Vol. 1, 1995, pp. 754-7 Vol 1.

[16] Reiser, C. J. "Design and Implementation of a Sampling Swept Time Delay Short Pulse (SSTDSP) Wireless Channel Sounder For LMDS", Master's Thesis, Department of Electrical and Computer Engineering, Virginia Polytechnic Institute and State University, 2001.

[17] Sweeney, D. "The design of SSTDSP sounder " (Through private communication), Center for Wireless Communication at Virginia Tech, 2001.

[18] Anderson, H. R. Estimating 28 GHz LMDS Channel Dispersion in Urban Areas Using a Ray-Tracing Propagation Model, *IEEE MTT-S International Topical Symposium on Technologies for Wireless Application*, 1999.

[19] Maurer, J., Didascalou, D., Engels, V., and Wiesbeck, W. Wideband Wave Propagation Measurements for Local Multipoint Distribution Services (LMDS) at 26 GHz, *Vehicular Technology Conference* Fall 2000. IEEE Part vol. 4, 2000, pp. 1902-8 vol. 4.

[20] Ravi, D. V., and Soma, P. Model of Local Multipoint Distribution Service (LMDS) Channel at 27.4 GHz Millimeter Wave Bands. 1999 *Asia Pacific Microwave Conference*. IEEE Part Vol. 3, pp 702-5, vol.

[21] Papazian, P. B., Hufford, G. A., Achatz, R. J., Hoffman R. Study of the Local Multipoint Distribution Service Radio Channel. *IEEE Transactions on Broadcasting*, Vol 43, No.2, June 1997.

[22] Chavero, M, Polo V., Ramos, F, and Marti, J. Impact of Vegetation On the Performance of 28 GHz LMDS Transmission. *IEEE MTT-S Digest*, Part Vol. 3, pp. 1063-6, 1999.

[23] Briso-Rodriguez, C., Vazquez-Castro, M. A., Alonso-Montes, J. E. 28GHz LMDS Channel Measurements and Modeling for Parameterized Urban Environments. *IEEE MTT-S Digest*, pp 2207-2210, 2001.

Appendix A. Scattering Model

This model is a combination of the two ray model, scattering loss factor, and radar cross section model for scattering. The model is used to calculate power delay profile in the radio channel.

A.1 Scattered E-field

The scattering model developed in this study is a modification of the two ray model. Instead of assuming that the reflected E-field is single ray E-field emanating from the specular reflection point, as described in Section 1.2, the reflected E-field has a lobe pattern as shown in Figure A.1. The energy from different points on the reflecting surface will reach the receiver with different amplitude and phase. Since

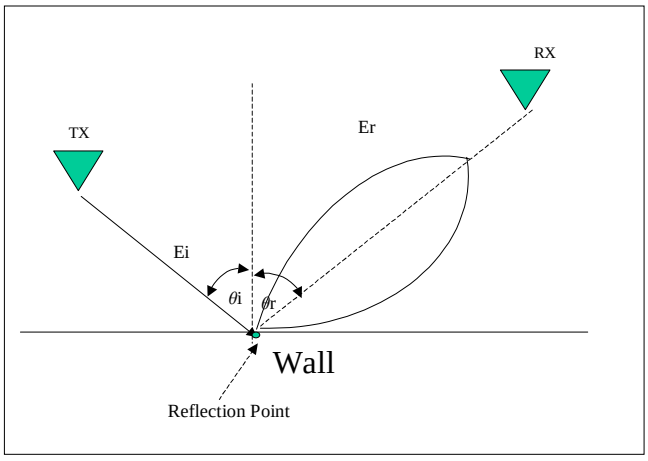

Figure A.1 Lobe shape E-Field

the energy is assumed to scatter with a lobe shaped pattern, the scattered E-field reaching the receiver can be calculated as

$$E_s = E_r \cdot \cos^n \phi \qquad \text{(A.1)}$$

for each scattered point. Angle ϕ is the angle between the specular direction and the direction from the reflection point to the receiving antenna (Figure A.2). As exponential *n* gets smaller the lobe shape E-field becomes bigger and diffuse scattering becomes more. On the other hand, as exponential n gets bigger, the lobe shape becomes smaller and becomes more like the specular E-field (Figure A.3). In the analytical model, the scattering loss factor is taken into account to calculate the

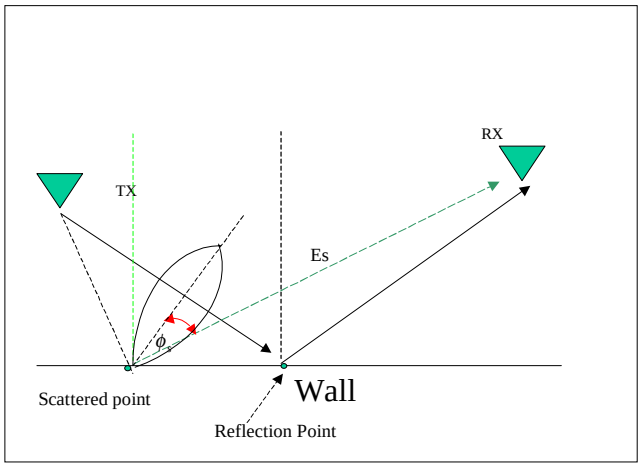

Figure A.2 Scattered E-field

reflected E-field. Therefore the reflected E-field is a product of the reflection coefficient (Γ), rough surface scattering loss factor (ρ), and incident E-field (E_i):

$$E_r = \Gamma \cdot \rho \cdot E_i \qquad \text{(A.2)}$$

Equations for calculating the reflection coefficient are Equations 1.7 and 1.8 in Chapter 1 and the rough surface scattering loss factor equation is Equation 1.15.

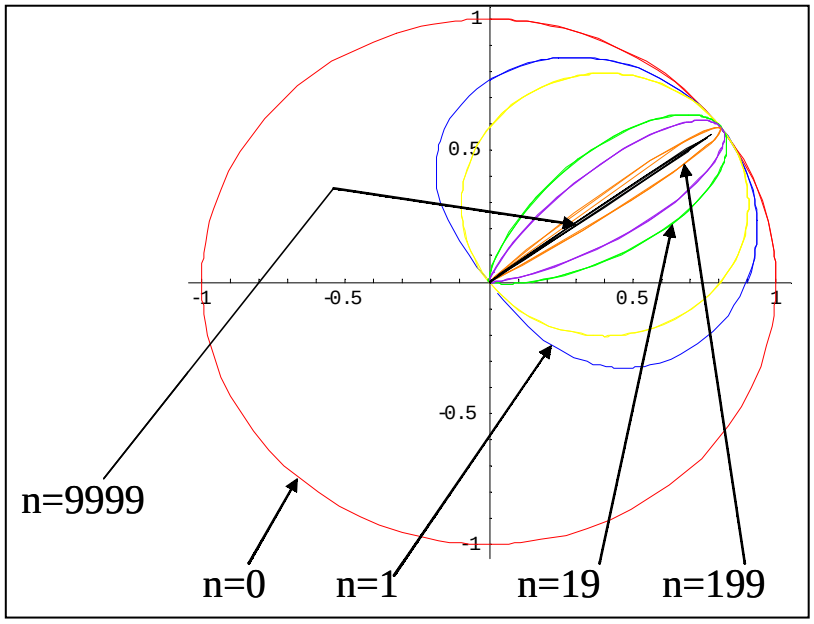

Figure A.3 Exponential n power

The magnitude of the incident E-field in free space from the transmitter is defined as follows [1]:

$$|E_i| = \sqrt{\eta_0 \frac{P_t G_t}{4\pi d^2}} \tag{A.3}$$

where P_t is the transmitter power, G_t is the transmitter gain, d is the distance from the transmitter to the reflection point, and η_0 is the intrinsic impedance of free space.

The phasor representation of the incident E-field in free space from the transmitter is defined [1] as:

$$E_i = |E_i| \cdot e^{-j(\omega \cdot d/c)} \tag{A.4}$$

where ω is the angular frequency, d is the distance from the transmitter to the reflection point, and c is the speed of light.

A.2 Received Power at Receiver

Power received at the receiver is calculated as power flux density incident on the reflection point (P_s) multiplied by the inverse squared loss ($1/[4\pi disRX^2]$), the receiver antenna aperture (A_e) and radar cross section area (RCS):

$$P_r = P_s \cdot \frac{1}{4\pi \cdot disRX^2} \cdot A_e \cdot RCS \qquad (A.5)$$

where $P_s = \frac{|E_s|^2}{\eta_0}$, $A_e = \frac{G_r \lambda^2}{4\pi}$ and disRX is the distance from the reflection point to the receiver (G_r as the receiver antenna gain and λ is the wave length at the

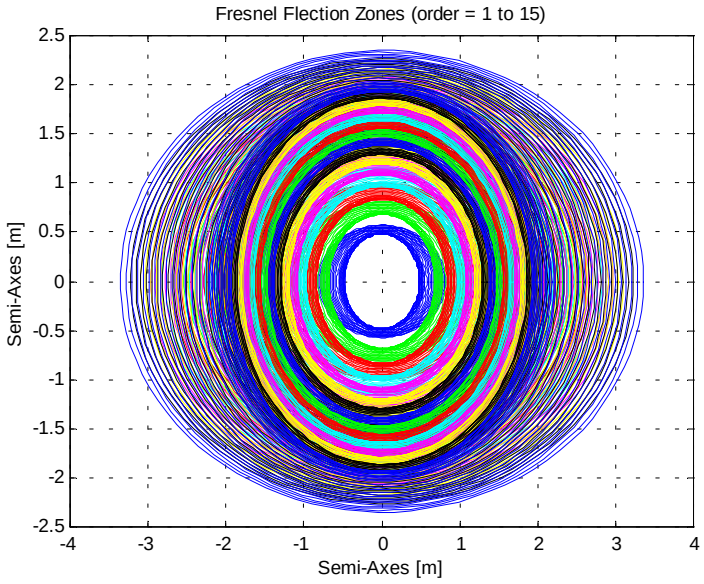

FigureA.4 Fresnel reflection zones (n = up to 15)

transmission frequency). This equation is similar to the radar cross section model described in Chapter 1.

In this model, the radar cross section area is estimated as the Fresnel

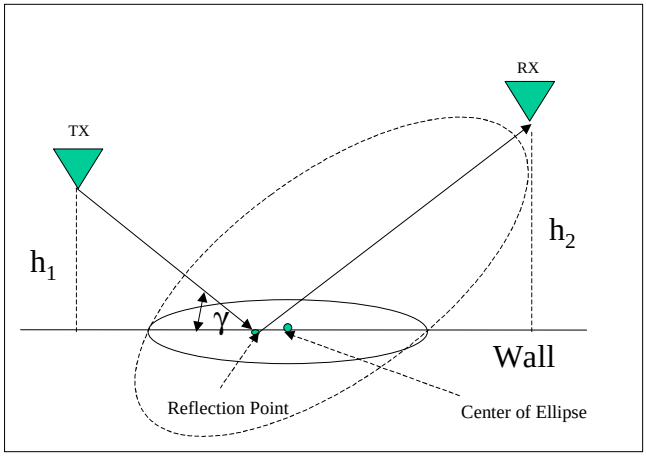

Figure A 5 Fresnel reflection zone geometry

reflection zone with zone order (*n*) as 15. The reason of choosing the zone order as 15 is because all the zones seem to converge as the order gets bigger. (Figure A.4). The Fresnel reflection zone is developed based on the same process that the Fresnel zone is defined. According to Histov [2], "Fresnel zones in case of reflection from plane earth serve to estimate the shape and size of ground region that is most significant for the reflected radio waves. There are elliptical zones with dimensions that for a given wavelength depend on the distance between the transmitter and receiver and the heights of their antennas." A Fresnel reflection zone is illustrated in Figure A.5. Assuming that the reflecting wall is a plane similar to ground, the

Fresnel reflection zone therefore is used as the reflection cross-section area in the analytical model.

To calculate the Fresnel reflection zone, the elliptical semi-axes need to be estimated. These calculations depend on antenna heights (h_1 as transmitter antenna height and h_2 as receiver antenna height) over the ground plane and equations are developed for three different cases [2]:

Case 1 ($h_1 << h_2$)

$$x_{on} \cong h_1 \cot\gamma \left(1 + \frac{n}{2h_1 \sin\gamma}\right) \tag{A.6}$$

$$a_n \cong \frac{1}{\sin\gamma}\sqrt{\frac{n\lambda h_1}{\sin\gamma}\left(1 + \frac{n\lambda}{4h_1 \sin\gamma}\right)} \tag{A.7}$$

$$b_n \cong a_n \sin\gamma \tag{A.8}$$

Case 2 ($h_1 >> h_2$)

$$x_{on} \cong h_2 \cot\gamma \left(1 + \frac{n}{2h_2 \sin\gamma}\right) \tag{A.9}$$

$$a_n \cong \frac{1}{\sin\gamma}\sqrt{\frac{n\lambda h_2}{\sin\gamma}\left(1 + \frac{n\lambda}{4h_2 \sin\gamma}\right)} \tag{A.10}$$

$$b_n \cong a_n \sin\gamma \tag{A.11}$$

Case 3 ($h_1 = h_2$)

$$x_{on} \cong h \cot\gamma \tag{A.12}$$

$$a_n \cong \frac{1}{\sin\gamma}\sqrt{\frac{n\lambda h}{2\sin\gamma}} \tag{A.13}$$

$$b_n \cong a_n \sin\gamma \tag{A.14}$$

where x_{on} is the center of the n^{th} ellipse measured from the coordinate origin O and its semi-axes are a_n and b_n. In the analytical model, antenna heights in the equation will be replaced by the distance from the transmitter and the distance from the receiver to the reflection point on the wall.

In the process of developing this model, it was found that the scattered E-field might arrive at the receiver at the same delayed time compared with the LOS E-field. Therefore power received at the receiver can be calculated as the following if there are two scattered E-fields arriving at the receiver at the same time:

$$\mathrm{P_r} = \left(\frac{\left|E_{s1}\right|^2 \cdot G_{r1}}{(4\pi disRX_1)^2} \cdot A_1 + \frac{\left|E_{s2}\right|^2 \cdot G_{r2}}{(4\pi disRX_2)^2} \cdot A_2 \right) \cdot \frac{\lambda^2}{\eta_0} \tag{A.15}$$

A.3 Medium Parameters

To calculate the incident E-field, the reflected E-field and scattered E-field described in Sections 3.1 on limestone and brick wall, we need to include medium parameters such as permittivity, permeability and conductivity in the equations. It is difficult to find medium parameters for high frequencies such as those within the LMDS band in the literature. In this study we assumed that all the medium parameters are similar to those at 4 GHz. reported by Landron [3], as given in Table A.1.

Table A.1 Medium Parameters

Wall Type	Relative Permittivity, ϵ_r	Relative Permeability, μ_r	σ
			[S/m]
Limestone	7.51	0.95	0.03
Brick	4.44	0.99	0.01

Some constants in free space used in this simulation model include: permittivity (ϵ_0) $8.85 \cdot 10^{-12}$ [F/m]; permeability (μ_0), $4\pi \cdot 10^{-7}$ [H/m]; and intrinsic impedance of free space, (η_0); 120π. With all the parameters listed above and operating transmitting frequency, medium intrinsic impedance (η)can be calculated with Equation 1.6.

A.4 LMDS Radio Parameters Used in the Scattering Model

The LMDS radio used in this study is a Spectra Point radio donated by Motorola. The transmitter and receiver operate at 28 GHz band, and both have 90 degree antenna patterns with 12 dB maximum gain as well as vertical polarization. The transmitter can transmit maximum one-watt power. The antenna pattern used in the simulation model was the pattern measured in Section 3.1.3.

A.5 Power Delay Profile

The aim of the model is to estimate the exponent, n in Equation A.1 to estimate the scattered power from different reflection wall. With all the equations listed above, Matlab programs were used to model power delay profile with a specific set-up. Example of power delay profiles of brick wall with incident angle as 15^o and *d1, d2* equal to 6m are shown in Figures A.6.

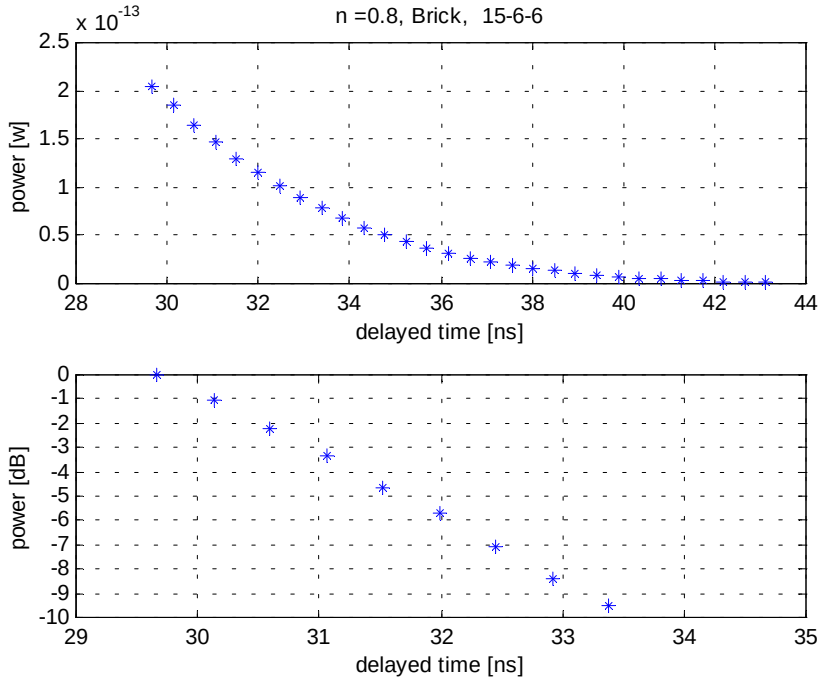

Figure A.5 Power delay profile with n = 0.8 for scattered E

The aim of the model is to estimate the exponent, n, in the equation 3.1 in order to estimate the scattered power from different reflection wall. With all these equations, A Matlab program listed in the end of this document can be used to model the power delay profile taken in a specific setting with different type of wall, angle and distance from the wall. Three power delay profiles which are for limestone set-up as incident angle, 5 degrees, *d1*and *d2* equal to 6 m, are shown in Figures A.5.

A.6 Comparison of Field Data and the Scattering Model

For each set of field collected data mentioned in Table 4.1, the Matlab codes based on the scattering model was used to find the exponential power *n* which was used to create the most similar power delay profile to match the raw data power

Table A.2 Comparison of Measured and Simulated Excess Pulse

Brick				Measurement					Simulation		difference	
				Pulse Width		Excess Pulse Duration		n	Excess Pulse Duration		(sim.-mea.)	
Case #	Angle	d1	d2	3 dB	10 dB	3dB	10dB		3 dB	10 dB	3 dB	10 dB
	[deg]	[m]	[m]	[ns]	[ns]	[ns]	[ns]		[ns]	[ns]	[ns]	[ns]
1	5	6	6	4	8.5	1	1	0.8	1	3.5	0	2.5
4		9	9	6	11	3	3.5	0.5	2	7	-1	3.5
5	10	6	6	4.5	9	1.5	1.5	0.5	1.5	4.5	0	3
8		9	9	4	8	1	0.5	1	1.5	4.5	0.5	4
9	15	6	6	4	11	1	3.5	0.8	1.5	4	0.5	0.5
12		9	9	3.5	6	0.5	-1.5	1	1.5	4.5	1	6
13	30	6	6	4	8	1	0.5	1	1.5	3.25	0.5	2.75
16		9	9	4	7	1	-0.5	1	2	5	1	5.5
17	45	6	6	3.5	10	0.5	2.5	1	1	3	0.5	0.5
20		9	9	7.5	10	4.5	2.5	0.5	4.5	7.5	0	5
			Ave=	4.5	8.9			0.8	1.8	4.7	0.3	3.3
			SD =	1.3	1.7			0.2	1.0	1.5	0.6	1.9

Limestone				Measurement					Simulation		Difference	
				Pulse Width		Excess Pulse Duration		n	Excess Pulse Duration		(sim.-mea.)	
Case #	Angle	d1	d2	3 dB	10 dB	3dB	10dB		3 dB	10 dB	3 dB	10 dB
	[deg]	[m]	[m]	[ns]	[ns]	[ns]	[ns]		[ns]	[ns]	[ns]	[ns]
1	5	6	6	2	3	-1	-4.5	1	0	0	1	4.5
4		9	9	8	13	5	5.5	0	3	11	-2	5.5
5	10	6	6	4	9	1	1.5	0.8	1.5	3.5	0.5	2
8		9	9	4	6	1	-1.5	1	1.5	3.5	0.5	5
9	15	6	6	4	9	1	1.5	1	1	2	0	0.5
12		9	9	4	11	1	3.5	0.8	1.5	5.5	0.5	2
13	30	6	6	4	11	1	3.5	0.8	1.5	3.5	0.5	0
16		9	9	4	10	1	2.5	1	2	5	1	2.5
17	45	6	6	6	8	3	0.5	0.5	3	4.5	0	4
20		9	9	8	10	5	2.5	0.5	3.5	7.5	-1.5	5
			Ave=	4.8	9.0			0.7	1.9	4.6	0.1	3.1
			SD =	1.9	2.8			0.3	1.1	3.0	1.0	2.0

delay profile. The results value of *n* and difference between the reflected excess pulse duration of measured raw data and of simulation for each set up are summarized in Table A.2.

Figure A.7 and Figure A.8 show the comparison of measured excess pulse width duration and simulation pulse width duration at –3dB level for brick wall and limestone wall.

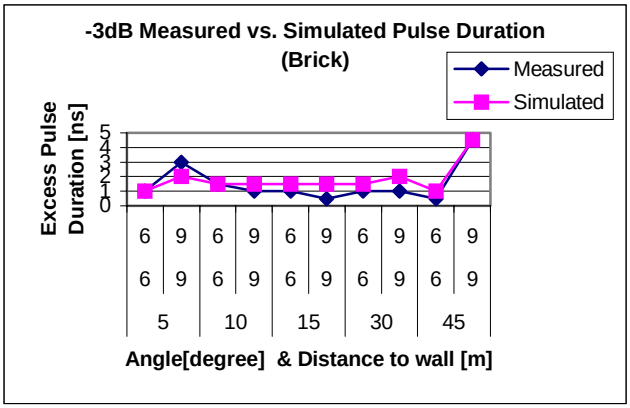

Figure A.7 Excess pulse width comparison (brick)

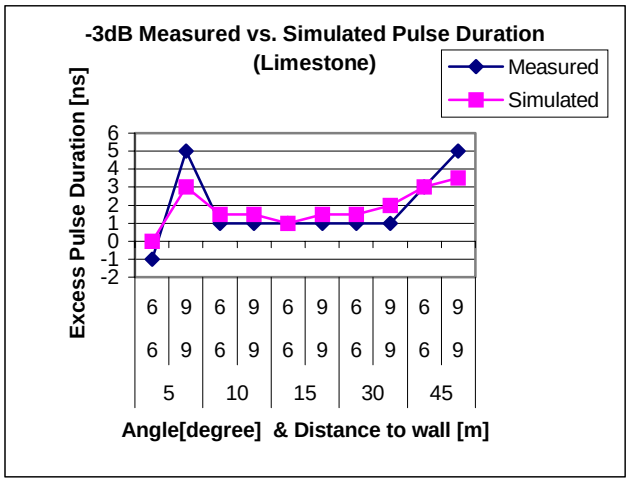

Figure A.8 Excess pulse width comparison (limestone)

A.7 Matlab codes to calculate and plot power delay profile

The following set of codes is an example of how calculation is used to approximate exponential power n for a set-up of brick wall measurement.

```
%Thesis simulation 02/09/03
%Limestone simulation based on the data collected for Thesis

%Calculation of Ps with antenna gain
clear all
subplot(2,1,1)
hold off
subplot(2,1,2)
hold off
%load antenna pattern file: In this file Gain is normalized
load antenna_pattern
%costants:f, lamda, permittivity(eps), conductance(sigma),
permeability(mu), refraction index(n2), intrinsic impedance(eta)
f = 28*10^9;
lamda = 2.998*10^8/f;
eps0 = 8.85*10^-12; %F/m
epsR = 7.51;
mu0 = 4*pi*10^-7; %H/m
muR = 0.95;%0.95
sigma = 0.03;
eps2 = eps0*epsR;
w = 2*pi*f;
eta0 = 120*pi;
eta2 = (j*w*mu0*muR/(sigma+j*w*eps0*epsR))^0.5;
n2 = 120*pi/eta2; %refraction index
sdh = 0.025; %2.5cm

%constants: Pt, Gt, Gr
Pt = 10^((30-30)/10); %30 dBm converted to watt
Gt = 10^(12/10); %12 dB
Gr = 10^(12/10); %12 dB

%data for limestone
thetadeg = [5 5 5 5 10 10 10 10 15 15 15 15 30 30 30 30 45 45 45 45
60 60 60 60];
d1 = [6 3 9 9 6 3 9 9 6 3 9 9 6 3 9 9 6 6 9 9 15 15 18 21];
d2 = [6 9 3 9 6 9 3 9 6 9 3 9 6 9 3 9 6 9 6 9 15 18 15 21];

theta = thetadeg/180*pi;

%calculate LOS distance
dLOS = (d1.^2+d2.^2-2.*d1.*d2.*cos(2.*theta)).^0.5;

%calculate tansmitter and receiver distance etc.
Yt = d1.*sin(pi/2-theta);
```

```
Xt = 0;
Yr = d2.*sin(pi/2-theta);
Xr = d1.*cos(pi/2-theta)+d2.*cos(pi/2-theta);% total distance from
TX perpendicular point to RX perpendicular point
%input sample number

sampleNo =30

%input n power
npower =0.5

%initilize matrix
deginphi_matrix = zeros(sampleNo,2);
inphi_matrix = zeros(sampleNo,2);
refP_matrix = zeros(sampleNo,2);
X1_matrix = zeros(sampleNo,2);
X2_matrix = zeros(sampleNo,2);

i = 20; %just to look at one set of data
dlos = dLOS(i);

%
%
for N = 1:sampleNo

stepsizeD =50*lamda*(N-1);%size of d step [meter]
totalD = (d1(i)+d2(i)+stepsizeD)*1.000000000001; %to fool the math
of matlab in order to get rid of complex number root due to round
off
%find two X1 that have the same delay time
syms X1 YT YR D1 D2 XR;
eq1 = (X1^2+YT^2)^(1/2) + ((XR-X1)^2+YR^2)^(1/2) -totalD;
eq2 = YT-Yt(i);
eq3 = YR-Yr(i);
eq4 = D1-d1(i);
eq5 = D2-d2(i);
eq6 = XR-Xr(i);
S = solve(eq1,eq2,eq3,eq4,eq5,eq6);


%if size(S.X1)==1
 %  X1_matrix(1,1)=double(S.X1)
  % X1_matrix(1,2)=double(S.X1)
   %X1=X1_matrix(N,:)
%end

%convert variables to row
YT = double(S.YT)'; %distance of TX to the wall
YR = double(S.YR)'; %distance of RX to the wall
XR = double(S.XR)'; %total distance of x
X1 = double(S.X1)';%TX perpendicular point to reflection point
X2 = double(S.XR)'-X1; %RX perpendicular point to reflection point
D1 = double(S.D1)'; %distance of TX to 2 ray reflection point
D2 = double(S.D2)'; %distance of RX to 2 ray reflection point

   %sorting X1 and X2
   if X1(1)>X1(2)
```

```
   large = X1(1);
   small = X1(2);
   X1(1) = small;
   X1(2) = large;
   end

   X2 = XR-X1;


%%%%%%%%%%%%%%%%%%%%%%%%%%%%%%%%%%%%%%%%%%%%%%%%%%%%%%%%%%%%%%%%%%%%
%%%%%%%%%%%%%%%%%%%%%%%%%%%%%%%%%%%%%%%%

%the following calculation is not limited to x range between TX
perpendicular point to RX perpendicular point


%%%%%%%%%%%%%%%%%%%%%%%%%%%%%%%%%%%%%%%%%%%%%%%%%%%%%%%%%%%%%%%%%%%%
%%%%%%%%%%%%%%%%%%%%%%%%%%%%%%%%%%%%%%%%%



   %calculate phi
   inphi = atan(X1./YT);
   deginphi = inphi/pi*180;
   phi = atan(X2./YR)-inphi;
   degphi = phi/pi*180;

   %convert varibles to matrixes with one row and 2 elements
   N2 = n2+zeros(1,2);
   SDH = sdh+zeros(1,2);
   ETA0 = eta0+zeros(1,2);
   PT = Pt+zeros(1,2);
   GT = Gt+zeros(1,2);
   DLOS = dlos+zeros(1,2);
   LAMDA = lamda+zeros(1,2);
   W = w+zeros(1,2);
   THETA = theta(i)+zeros(1,2);  %the two ray angle

   %calculate reflection coefficient / loss factor

   refE = (cos(inphi)-(N2.^2-sin(inphi).^2).^0.5)./...
          (cos(inphi)+(N2.^2-sin(inphi).^2).^0.5);%perpendicula or
horizontal reflection coefficient
   refH = ((N2.^2-sin(inphi).^2).^0.5-N2.^2.*cos(inphi))./...
          ((N2.^2-sin(inphi).^2).^0.5+N2.^2.*cos(inphi)); %Parallel
or vertical reflection coefficient
   roS = exp(-8*(pi*SDH.*cos(inphi)./lamda).^2).*...
      besseli(0,8*(pi*SDH.*cos(inphi)./lamda).^2);%reflection loss
factor

   %calculate distance to TX & RX
   disTX = (X1.^2+YT.^2).^0.5;   %distance of reflection point to TX
   disRX = (X2.^2+YR.^2).^0.5;   %distance of reflection point to RX

   %calculate  reflection cross section area major and minor axes
   %calculate garma
   m=15; %order of Fresnel zone
```

```
   garma = pi/2-inphi;
   deggarma = garma/pi*180;
    %calculate  reflection area major and minor axes
    if YT < YR
      major =
1./sin(garma).*(m.*LAMDA.*YT./sin(garma).*(1+m.*LAMDA./(4*YT.*sin(ga
rma)))).^0.5;
      minor = major.*sin(garma);
      elseif YT > YR
      major =
1./sin(garma).*(m.*LAMDA.*YR./sin(garma).*(1+m.*LAMDA./(4*YR.*sin(ga
rma)))).^0.5;
      minor = major.*sin(garma);
      else
      major = 1./sin(garma).*(m.*LAMDA.*YR./2/sin(garma)).^0.5;
      minor = major.*sin(garma);
    end
    area = pi.*major.*minor;

   %calculate antenna gain for each Ei
   phiT = inphi - THETA;
   degphiT = round(phiT./pi*180);

   angle = [-179:180];
   for m=1:2
   n = find(angle==degphiT(m));
   GainT(n) = 10^(new_gain_low(n)/10);
   GainTX(m) = GainT(n);
   end


   %calculate incident E and delatyed time
   Ei_abs = (ETA0.*PT.*GainTX./(4*pi.*disTX.^2)).^0.5;   %incident E
field magnitude
   Ei = Ei_abs.*exp(-j.*W.*(disTX)./(2.998*10^8)); %indident E field
phasor expression
   Td = (disTX+disRX-DLOS)./(2.998*10^8); %delayed time



   ErE = refE.*roS.*Ei; %reflected E field for Perpendicular
polarization
   ErH = refH.*roS.*Ei;


%%%%%%%%%%%%%%%%%%%%%%%%%%%%%%%%%%%%%%%%%%%%%%%%%%%%%%%%%%%%%%%%%%%%%%%
%%%

%%%%%%%%%%%%%%%%%%%%%%%%%%%%%%%%%%%%%%%%%%%%%%%%%%%%%%%%%%%%%%%%%%%%%%%
%%%%%
   % Varying npower will give you different Es value


   Es = ErE.*cos(phi).^npower; %scatted E field on the reflection
point
   %calculate received gain antenna aperture
```

```
 %first need to calculate antenna gain for each phiR
     phiR = atan(X2./YR)-THETA;


   degphiR = round(phiR./pi*180);
   for m=1:2
      n = find(angle==degphiR(m));
      GainR(n) = 10^(new_gain_low(n)/10);
      GainRX(m) = GainR(n);
   end

   %calculate power and delayed time in ns
   Es_abs = abs(Es);
   two_Ps = Es_abs.^2.*GainRX./((4*pi.*disRX).^2).*area;
   %power in Watt intrinsic impedance is included

    Ps_W = sum(two_Ps)*(lamda^2)/(120*pi);
    if N == 1
       Ps_max = Ps_W
    end

   Ps = 10*log(Ps_W/Ps_max);%normalized

   Td = Td*10^9; % Td in ns
   Td = Td(1);

   %plot each point
   subplot(2,1,1);
   plot(Td,Ps_W,'*');
   hold on
   title('n =0.5, Limestone 45-9-9')
   xlabel('delayed time [ns]');
   ylabel('power [w]');
   grid on;
   subplot(2,1,2);
   plot(Td,Ps,'*');
   hold on
   xlabel('delayed time [ns]');
   ylabel('power [dB]');
   axis([0 max(Td) -10 0])
   grid on;
end
```

A.8 References

[1] Rappaport, T. S. *Wireless Communications: Principles and Practice (2nd Ed).* Prentice Hall, NJ. 2002.

[2] Hristov, Hristo D. *Fresnel Zones: Wireless Links, Zone Plate Lenses and Antennas*. Artech House: Boston, 2000.

[3] Landron, O. Feuerstein, M. J., and Rappaport, T. S. In Situ Microwave Reflection Coefficient Measurements for Smooth and Rough Exterior Wall Surfaces. *IEEE Vehicular Technology Conference*, Secaucus, NJ, May 18-20, 1993.

Vita

Cindy Lin Dillard was born in Taiwan and came to the United States in 1984 to work on her first graduate degree in Education at Virginia Tech. Electrical Engineering is her second career development. Before coming back to Engineering school, she earned a PhD in Child Development in 1988 and has worked as an assistant professor at State University of New York at Geneseo (1988-1989) as well as an adjunct professor at Virginia Tech and New River Community College in the educational field for a number of years. Her specialties in wireless communication include Local Multiple Distribution Services (LMDS) radio system, RF circuit design, communication system design, and satellite communication. In her graduate studies, she is involved with a NSF research project to develop a LMDS wireless communication system for use in disaster and rescue areas. She has also spent a semester working at Luna Innovation as an intern in the fall of 2002. Her involvements with Luna include assisting senior engineers in designing and testing RF circuits, as well as proposal writing.